OPTICAL STUDIES OF RADIATION DAMAGE AND IMPURITIES IN $RbCdF_3$

By

RUO-LING HU

Bachelor of Science

Shanghai Institute of Mechanical Engineering

Shanghai, China

1966

Submitted to the Faculty of the Graduate College
of the Oklahoma State University
in partial fulfillment of the requirements
for the Degree of
MASTER OF SCIENCE
July, 1987

OPTICAL STUDIES OF RADIATION DAMAGE

AND IMPURITIES IN $RbCdF_3$

Thesis Approved:

W. A. Sibley

Thesis Adviser

Larry E. Halliburton

Paul W. Seathaver

Norman N. Durham

Dean of the Graduate College

ACKNOWLEDGEMENTS

It is a pleasure and good fortune to have studied in the Physics Department of Oklahoma State University.

The author is deeply grateful to her advisor, Dr. William A. Sibley, for his generous and patient guidance throughout this study. It is a great honour to work in his laboratory.

Her heartfelt gratitude is expressed to Dr. Paul Westhaus and Dr. Yoshiro Suzuki for their valuable assistance and many helpful discussions.

Appreciation is extended to Dr. L. E. Halliburton for his encouragement and various assistance during her graduate studies.

Thanks are expressed to Dr. Donald Yeh and Dr. Jorge Garcia, the members of Dr. Sibley's research group, for their friendly help and useful discussions.

Finally, acknowledgements are especially sent to her parents for their support, encouragement and patience, as well as taking charge of my only daughter since she was born.

TABLE OF CONTENTS

LIST OF TABLES

LIST OF FIGURES

CHAPTER I

INTRODUCTION

Investigation of the optical properties of solids is of great importance since materials are essential in the development of modern solid-state lasers and devices. Also this research extends our knowledge of solid-state physics and modern materials.

The laser field is fascinating in many ways[1]. The rapid development of modern laser devices has resulted in their wide application in scientific laboratories and in industry. For example, the newly developed tunable lasers which are based on color centers in alkali halide crystals now are used in research on fiber optics, molecular spectroscopy, and nonlinear optics. Obviously, the technical development of practical lasers is directly based on the progress of fundamental research in solid state physics. Therefore, people have become more aware of the significance of characterizing basic materials.

The characterization of fluoride crystals includes studies of the magnetic, thermal, optical, and mechanical properties. Color center physics[2] constitutes one of these fundamental areas. In this thesis, special attention is paid to radiation-induced changes in the optical

properties of both pure and divalent manganese doped $RbCdF_3$.

It is well known that two categories of defects exist in crystals:

(1) Point defects, which can be introduced by impurity doping[3], irradiation[4], additive coloration[5], electrolytic coloration[6], and ion implantation[7].

(2) Structural defects, such as dislocations which arise from stress and can be arranged in subgrain boundaries.

In the present study, emphasis is placed on point defects. Conceptually, the simplest of all point defects are isolated interstitials or vacancies. The interstitial is an ion or atom that occupies a position where no atom would exist in a perfect crystal. The vacancy is defined as the position where an ion or atom is missing from the perfect lattice structure. Point defects can be much more complicated than isolated vacancies and interstitials. The name "point defect" is used for any complex of simple defects which still has a fairly simple symmetry. Figure 1[2] illustrates typical point defects in a simple two-dimensional square lattice. Intrinsic defects involve only the rearrangement of ions of the perfect solid. Simple vacancies and interstitials are examples of intrinsic defects. Impurities are designated as extrinsic defects. Intrinsic vacancies or interstitials can move freely at sufficiently high temperatures and may associate with

impurities to form impurity-vacancy or impurity-interstitial complexes.

High energy irradiation can create point defects in all solid materials. Investigations of radiation damage in ionic crystals, particularly the alkali halides, have been carried out extensively[4,8-11]. The nature of the damage produced in this way depends on both the type of irradiation and material. The theoretical treatment of radiation damage consists of four parts which are described below:

(a) Interaction between radiation and matter

The interaction between the irradiating particle or photon and the solid may be thought of as two-body collisions between the incident particles and the constituent particles of the solid. The latter, having received energy by such a " primary event ", are called " primary particles ". A variety of processes are responsible for the loss of energy. The energy loss per unit path of a heavy particle at high energies can be written as[2]:

$$-(dE/dx) = (4\pi z^2 e^4 N_0 Z/mv^2) * \log \{[2mv^2/\sigma(1-B^2)] - B^2\}$$

where dE/dx is the energy loss in ergs per unit path length in centimeters, e and m are the electron charge and the rest mass, z and v are charge and velocity of the incident particle, N_0 is the atomic density of the crystal, Z is the number of "excitable" electrons per target atom, and σ is the average excitation potential of these electrons. The

ratio v/c is labeled B with c, the velocity of light.

(b) Radiation damage production

Energy transfer from the incident radiation to a primary particle causes it to leave its equilibrium lattice site and a defect is produced. If the primary knock-on carries sufficient kinetic energy with it, further defects can be created in a cascade-like manner. This damage production process is highly dynamical which may carry ions far from their initial site and can cause thermal spikes for a short time.

Of course, this is not the way defects are produced in highly ionic material. In these materials radiolysis occurs. The photochemical or radiolysis processes are those in which atomic or ionic defects are formed by a series of reactions beginning with an electronic excitation. There are three stages in such a process. First, an electronic excitation must occur. The energy lost by the radiation in causing an electronic excitation is capable of creating an electronic defect in the lattice. Second, the energy of the electronic defect must be converted into kinetic energy of a lattice ion in such a way that the ion is ejected from its normal site. Third, a route must exist for this lattice ion to move sufficiently far from its associated vacancy that a stable defect is formed.[12]

The most frequently studied point defect is the negative ion vacancy with a trapped electron (F-center). The correct structure for an F-center in alkali halides was

first proposed by de Boer [13] in 1937. F-centers are produced in most alkali halides by additive coloration in excess alkali metal vapor at sufficiently high temperatures or by irradiation with high energy photons or particles. Although the alkali halide F-center is the simplest center of all in concept and has been very widely studied, its properties are not always simple.

In this work we investigate F-centers, F_2-centers (M-centers) and other more complex F aggregates, as well as hole centers. Holes may be trapped to form color centers[14], which play a very important role in radiation damage.

When an electron is removed from a halide lattice ion in an ionization event, it leaves a hole behind. The resulting halide atom then combines with a nearest neighbor [110] halide ion which leads to a distortion in the surrounding lattice and thus creates a potential well in which a hole becomes " self-trapped ". The hole is equally shared in a covalent bond between the two halides. Therefore, a molecular-ion is established.

Daly and Mieher [15] have shown that the self-trapped hole (the V_k center) is an intrinsic defect in the sense that no ionic defects such as vacancies or interstitials are involved. The intrinsic V_k spectrum is independent of impurities, and for the most part it does not change substantially with the cation (see Figure 2a). There is only a very weak interaction between a V_k center and the

surrounding lattice. It is not the ionic structure but the electronic structure of the material which is altered by this defect.

The electronic structure of the H-center was first analyzed in detail by Kanzig and Woodruff [16] and is shown in Figure 2b. It was found that the fundamental interstitial produced in the alkali halides is a halide atom which bonded to several lattice halide ions. Thus, two halides share a single lattice site.

The fact that the vacancy and the interstitial are formed simultaneously by irradiation in alkali halides was first explained by Varley[17] and illustrated in Figure 3. He thought an incident photon could interact with a halide ion, and doubly ionize it, leaving it positively charged. The positive halide ion, located in the field of the six nearest neighbor positive alkali ions, would be highly unstable and the resulting motion of the neighboring ions could result in the ejection of the positive halide ion into an interstitial position. Because of the strong electron affinity of the positive halide ion, it would quickly trap an electron to become an atom and form the H center. The resulting halide-ion vacancy could then trap an electron to form an F center. Now we know that double ionization does not occur, and it has become clear that the creation of the F-H pair arises from the excited states of the exciton which is created when an $X_2^-(V_k)$ center, formed under ionizing radiation, traps an electron[18-23]. The

electronic structure of the self-trapped exciton including the higher excited states has been reviewed in detail by Itoh,[18] Williams and Kabler,[19,20] Toyozawa,[21] and others.[22-25] When a $X_2^-(V_k)$ center traps an electron in its highest bond orbital, there is a de-excitation to the lower lying levels. If the electron is de-excited to the $1s\sigma_g$ orbital π luminescence is emitted. If it is de-excited to the $2s\sigma_g$ orbital σ luminescence is emitted. It is known that the recombination of an H-center with an F-center emits π luminescence but not σ luminescence. This suggests that F-H pair production state is enegetically intermediate between the $1s\sigma_g$ and $2s\sigma_g$.

Measurements of the build-up time of F-centers and of π luminescence from excitation with picosecond lasers have been made.[26-29] This research has resulted in a much better understanding of the F-H production mechanism. For example, the delay in the formation of F-centers after an electron-hole event, is typically about 10 picoseconds. The decay of transient F-H centers occurs within about 40 ms.[30] It is also known that in the F-H production process impurities can play a major role. For example, a number of years ago it was discovered that trace impurities of Pb^{2+} in KCl can suppress the room temperature radiation damage considerably.[31] Lately, Tanimura and Okada[32] have shown that the addition of Na^+ to KBr also greatly suppresses the creation of F-centers. It appears in this latter case that the exciton energy is localized at the impurities which help

form perturbed self-trapped excitons and that the transformation yield from these perturbed self-trapped excitons into F-H pairs is very low.

In order for F- and H-centers to be stabilized, there must be defect mobility and defect aggregation or trapping. Ultimately it is these latter two processes that determine the total stable coloration of a crystal. For example, the research by Williams, et al.,[30] on transient absorption and luminescence in irradiated MgF_2 shows quite clearly that many more defects are formed initially than can be stabilized. They observe that at 5-10 K an F-H pair is created with energy expenditure of about 30 eV, whereas 4×10^5 eV is required to produce a <u>stable</u> F-H center pair. This implies, of course, that in most materials whether alkali halides or complex alkali earth halides, the production of F-H pairs is highly efficient, but it is the mobility and trapping of these defects that result in the total <u>stable</u> coloration in the crystal.

(c) Annealing

In general radiation produced defects are not stable. Annealing can occur. One has to distinguish between the instantaneous annealing regardless of the temperature, and the metastability which leads to annealing only at sufficiently high temperature. The nature and amount of damage may be strongly temperature-dependent.

(d) Property changes

Defects can be observed in direct ways through tools such as electron microscopy, but usually they are detected by their influence on the structure-sensitive properties of the samples.

Radiation defects are usually identified by their optical properties. The alkali halide crystals have been the subject of considerable color center research aimed at understanding the effect of ionizing radiation on the solid state.

These crystals have been subjected to different types of radiations (electrons, protons, neutrons, x-ray, gamma ray, and ultraviolet photons) over a wide range of temperature. Detectable radiation damage in the form of isolated, as well as clustered, vacancies and interstitials have been identified by numerous optical investigations.

Since fluoride materials have the qualities which make them applicable for laser devices, it is important to study the radiation damage processes in this material. $RbCdF_3$ crystals have a lattice constant of 4.3999 Å and a cubic perovskite structure which has the symmetry group O_h^1. In the unit cell the rubidium ions are at sites (0, 0, 0), cadmium ions at (1/2, 1/2, 1/2) and fluorine ions at (1/2, 1/2, 0), (1/2, 0, 1/2), and (0, 1/2, 1/2). Figure 4 shows the crystal structure in the cubic phase above T_c (T_c = 124 K). The phase transition from the cubic (O_h^1) to tetragonal (D_{18}^{4h}) symmetry is characterized by a rotation of the CdF_6-octahedra around one of their fourfold axes, which becomes

the tetragonal axis.[33-35] Crystals can be doped with Mn^{2+} ions which substitute for Cd^{2+} ions. The ionic radius of Mn^{2+} is about 20% smaller than that of Cd^{2+}.[36] The nearest-neighbor distance between fluorine and cation, R_{nn}, is 2.2 Å. The work of Williams, et al.[30] suggests that we might expect to find F center absorption at about 4.2 eV, H center absorption around 4.1 eV and $X_2^-(V_k)$ center absorption near 3.9 eV as shown in Figure 5. In this research we will identify the F, H and V_k band absorption in $RbCdF_3$ and discuss the production of these defects by ionizing irradiation. In addition the emission data from Mn^{2+} and Cr^{3+} ions in $RbCdF_3$ will be presented.

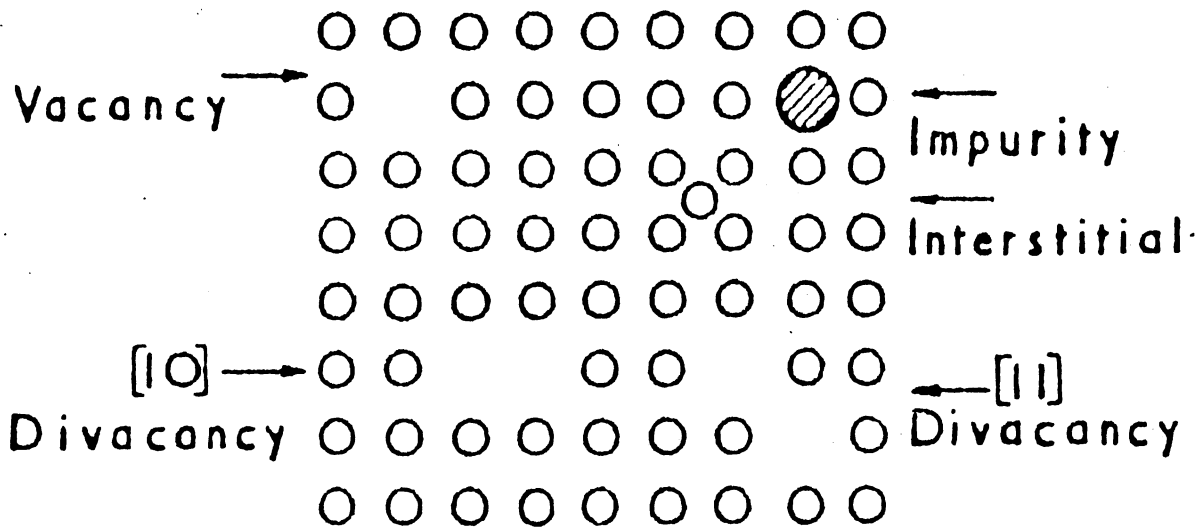

Figure 1. Point defects in a two-dimensional simple square lattice

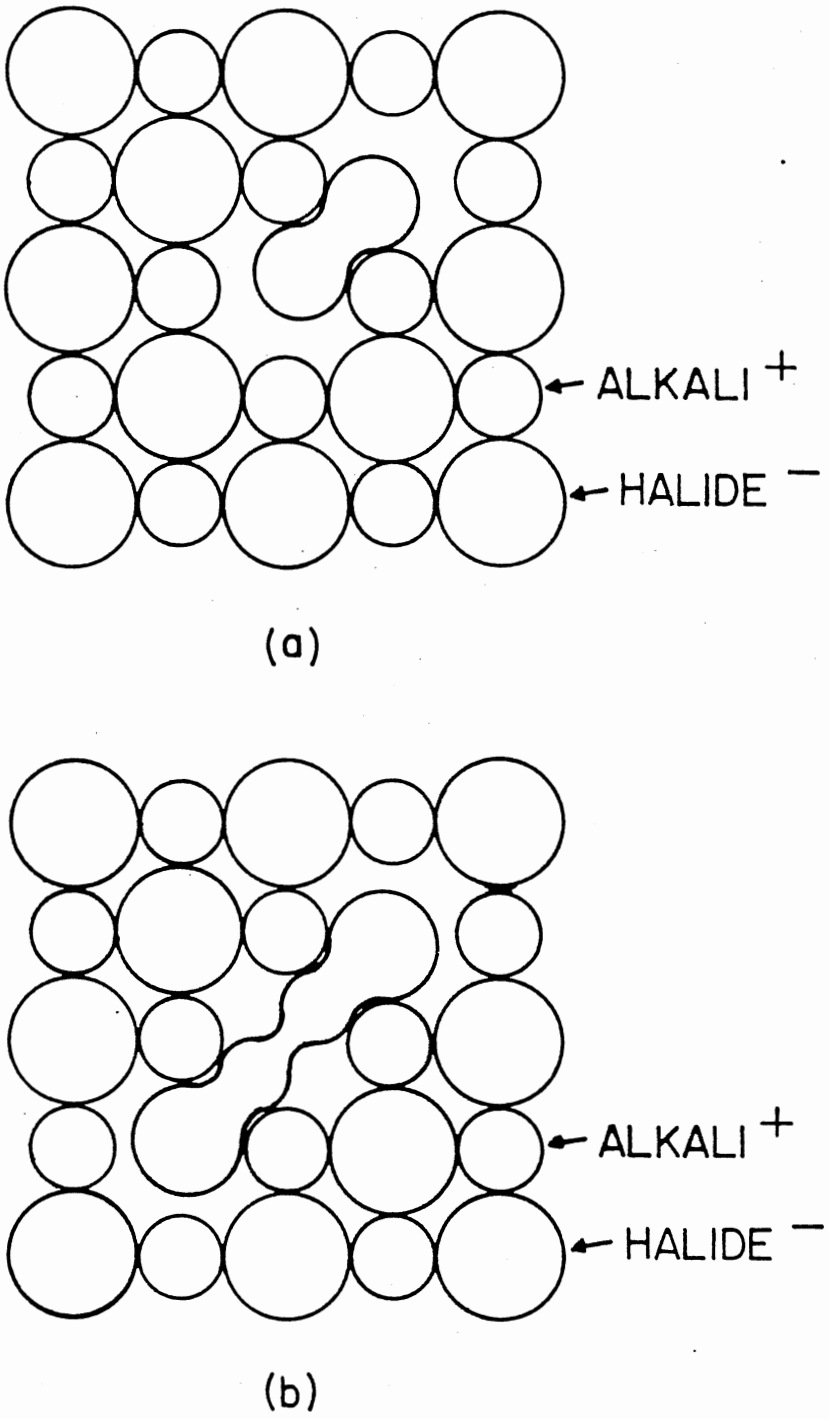

Figure 2. The structure of the (a) V_k^- center and (b) H center in the alkale halides

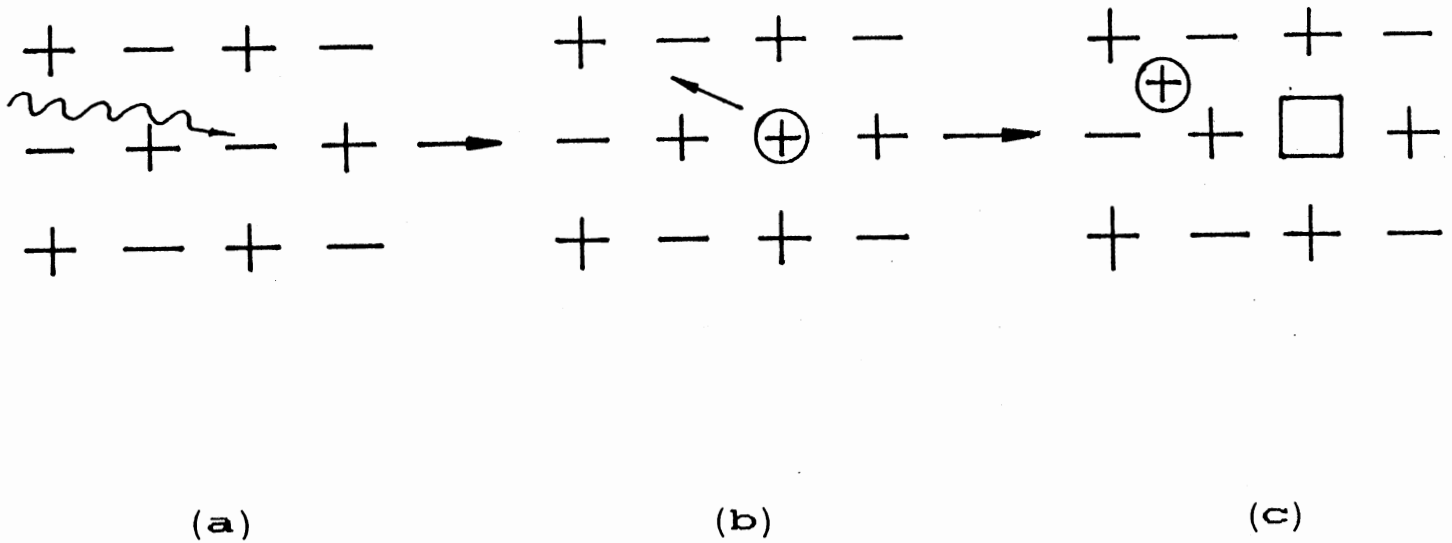

Figure 3. Schematic representation of the Varley mechanism of F-H defects formation

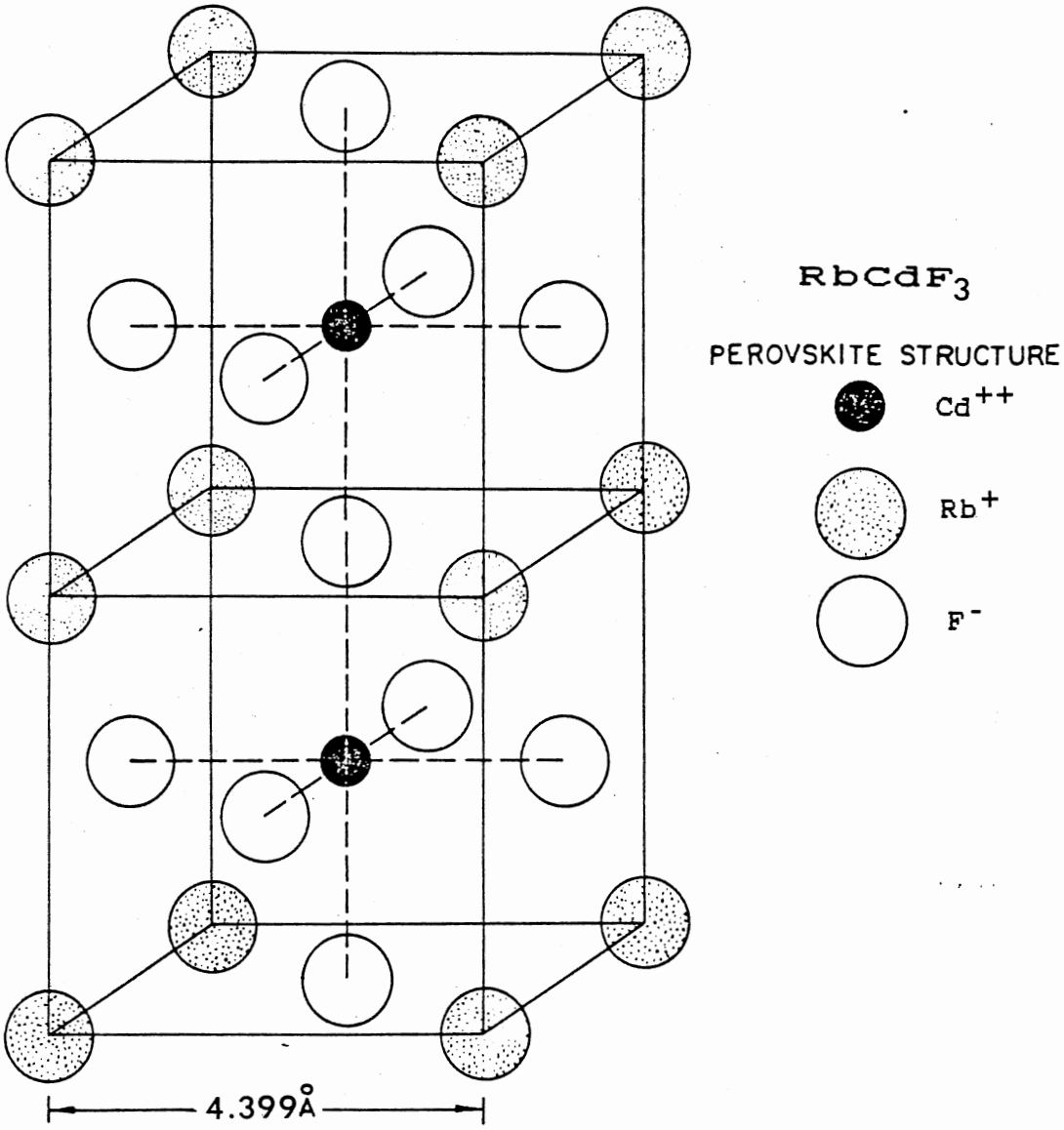

Figure 4. Two unit cells for $RbCdF_3$

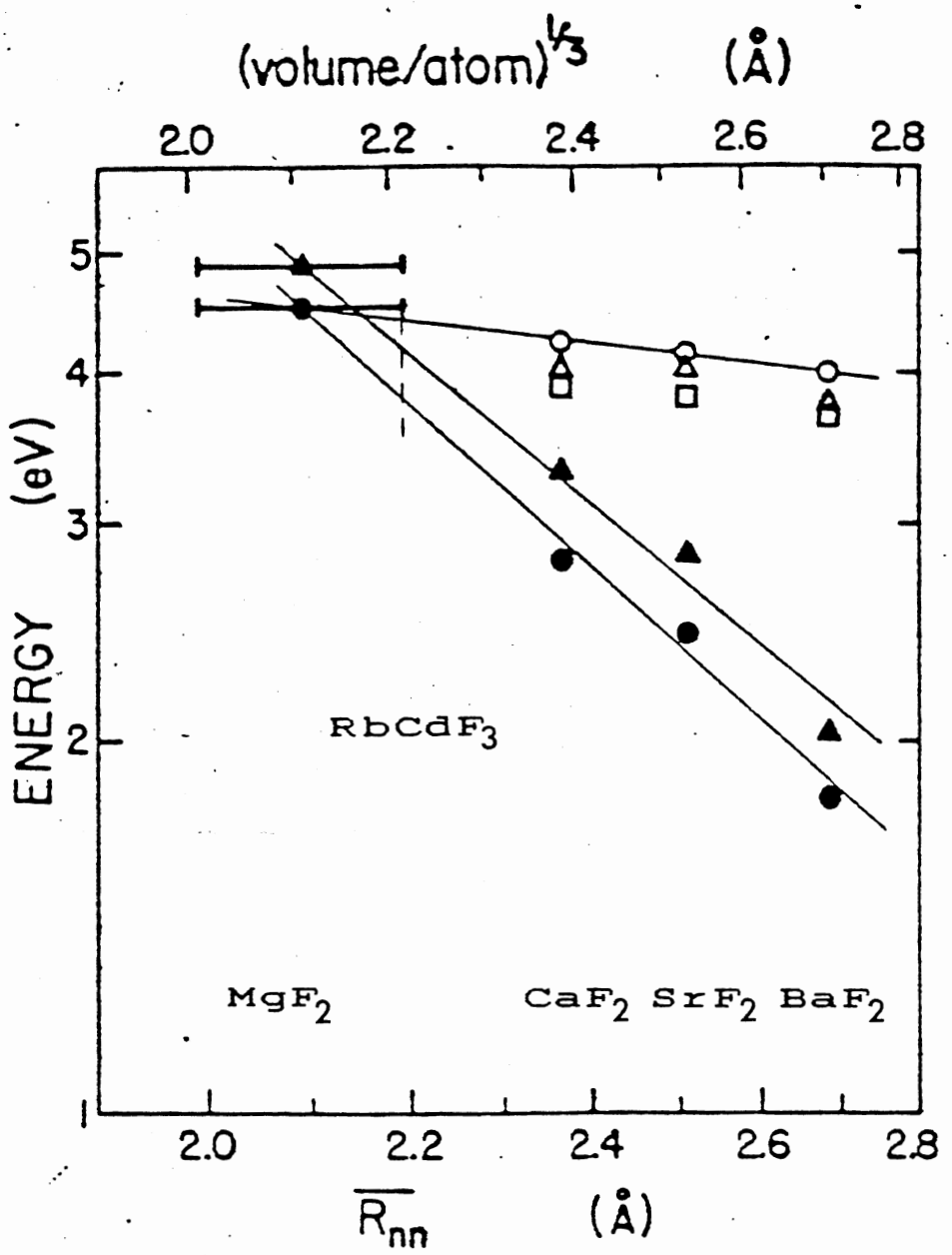

Figure 5. A plot of peak energies of absorption bands for F (▲), H (□) and V_k (△) centers vs. lattice parameter

CHRPTER II

EXPERIMENTAL EQUIPMENT AND PROCEDURES

Preparation of samples

The $RbCdF_3:Mn^{2+}$ and $RbCdF_3:Cr^{3+}$ crystals used in this study came from Professor Martin Spaeth at the UNIVERSITAT-GESAMTHOCHSCHULE-PADERBORN. Another undoped $RbCdF_3$ crystal was supplied by Dr. M. Shinn. The manganese-doped crystal contains 0.3 mol.% MnF_2 and the chromium-doped crystal contains 0.003 mol.% CrF_3. These concentrations were used to calculate the oscillator strengths of the observed Mn^{2+} optical transitions in the crystals.

The crystals were cut using an IMANCO Macrotome diamond saw. Surfaces were then polished by hand lapping on successively finer sheets of abrasives obtained from Buehler Ltd. The final polishing was done with 3 micron grit in ethanol.

Optical measurements

The optical absorption was detected by a Perkin-Elmer 330 Spectrophotometer which is a double-beam system comparing the absorption in any given sample to a reference. Basically the optical absorption in a homogeneous passive material can be understood in simple terms. The attenuation

of light passing through a material of thickness d (cm) is given by the expression

$$I = I_0 \exp(-\alpha d)$$

where I_0-- Intensity of light beam entering sample (incident beam)

I -- Intensity of light beam leaving sample

α -- Absorption coefficient expressed in units of inverse centimeters (cm^{-1})

The system records optical density as a function of wavelength covering a range of 200 nanometers to 2.5 microns.

The optical density is defined as

$$O.D = \log_{10} (I_0 / I)$$

The absorption coefficient is related to the optical density by the relation:

$$\alpha = \ln (I_0 / I) / d = (2.303)\ O.D. / d\ (cm^{-1})$$

Normally, α is plotted against photon energy or wavelength. For nominal concentrations of defects, the concentration of a color center is proportional to the optical density.

Excitation and emission spectra and lifetime measurements were performed by the system shown schematically in Figure 6. A 300 Watt short-arc Xenon lamp from Illumination Industries Inc. was used as the exciting

light source which was focused by quartz lenses on the slit of a 22 cm Minimate monochromator from Spex Industries Inc. The monochromator is controlled by a compudrive Spex Model CD2. Various gratings can be used in the Minimate. In this study two gratings were used. One grating has 1200 grooves with a reciprocal dispersion of 4 nm/mm blazed at 300 nm for the range from about 200 nm to about 900 nm. The other is a 600 groove grating blazed at 750 nm with a dispersion of 8 nm/mm, used over the range between 400 nm to about 1500 nm. The exciting light passed through both the 22 cm Minimate Spex and a suitable filter when necessary. Quartz lenses focused the light onto the center of the sample which was rotated about 20° from incident light to minimize reflection of the exciting light into the detection system. Care was excercised to reduce the scattered light entering the emission monochromator. The fluorescense was passed through a filter which reduced the exciting light and focused with calcium fluoride lenses onto the slit of a 0.8 m Spex 1702 monochromator controlled by a Compudrive 770 (Spex). The monochromator has a 600 gr/mm grating blazed at 1600 nm with a reciprocal dispersion of 2 nm/mm. The emerging light was routed to either a cooled PbS cell (Opto electronics OTC-22-53TXX) or photomultiplier tube (PMT) (RCA C31034 or RCA 7102). The 7102 tube is used for measurements near 1 um and is normally cooled with dry ice. The other tube is used for visible and ultraviolet light, and is cooled to about $-30^{\circ}C$ with a Pacific Photometric Model 33

thermoelectric cooler. The cooling reduces the noise (dark current). For D.C. measurements, the output signal of the photomultiplier tube was amplified by a Keithley Model 427 current amplifier. For A.C. measurement, the output signal of the PMT was preamplified by a Keithley Model 427 current amplifier and processed by a lock-in amplifier. The reference signal was provided by chopping the light which is detected by a phototransistor placed at the edge of the excitation light beam. The chopper can be controlled from 5 Hz to 700 Hz. When the PbS cell is used preamplification is performed by a Keithly Model 103A Nanovolt Amplifier. High voltage for the phototube is provided by a Fluke Model 412A High Voltage Power Supply, and for the PbS detector by a Fluke Model 301E precision DC power supply which can produce 145 volts smoothed by a filtering circuit. The output of amplified signal either from the 427 current amplifier for D.C. measurement or from the lock-in amplifier may be displayed on a Houston Instruments 2000 X-Y recorder and routed to a Hewlett-Packard Model 3455A digital voltmeter which is interfaced to a Hewlett-Packard Model 85 microcomputer. This allows excitation or emission spectra to be recorded on disc for further processing.

Lifetime measurements were made by using a Nicolet Model 1070 signal averager. When the signal is weak, it is possible to average over many scans by storing the information in a Nicolet Model 1070 Signal Averager. The signal-to-noise ratio of the emission signal goes as the

square root of the number of scans. The stored signal as a function of time is displayed on an oscilloscope, and may be stored on the HP-85 for analysis, or plotted to the X-Y recorder. The Nicolet is limited by its own electronics to dwell times on the order of 10 μs, but this can be overcome by using a Biomation Model 610B Transient Recorder to store single scans and then the data can be transferred to the Nicolet for averaging. The Biomation is capable of 100 nanosecond dwell times. The effective limit on our lifetime measurements is about 10 μs under optimum conditions.

Temperature dependence measurements

For low-temperature measurements, samples are mounted either in a liquid-nitrogen cryostat, or a CTI Cryodyne Cryocooler Model 21 SC. The Cryocooler incorporates a resistance heater which allows temperature control within ±2 K over the range from 14 to 300 K. These units are equipped with a rotatable tail section with CaF_2 windows to allow both absorption and luminescence measurements. Sample temperature between 14 and 300 K can be held accurately for long periods by balancing the heat input from the internal resistance heater against the removal of heat by the refrigerator. The sample temperature is measured to ±2 K by means of a thermocouple consisting of #36 gauge gold; 0.7 atomic % iron versus Chromel P wire, and the sample temperature in the Cryodyne Cryocooler could be varied continuously from 14 to 300 K by means of a 15 Watt

heater, and a temperature controller allowed the maintenance of any desired temperature for any desired period of time.

For measurements above room temperature the sample was enclosed in a copper holder with small windows for the entrance of excitation light and the exit of the fluorescence. A thermocouple was mounted directly on the sample to control the temperature within ±4 K.

Optical bleaching

Optical bleaching was carried out by illuminating the sample with light from a 100-watt high presure short arc mercury lamp (PEK112). The light was focused with quartz lenses and passed through an appropriate interference filter for required bleaching wavelength.

Thermal annealing

Two types of annealing experiments were utilized. For a continuous anneal, an immersion heater was used to slowly warm the sample while the absorption or luminescence were monitored by a Perkin-Elmer 330 spectrophotometer or luminescence detection apparatus. In the case of an isochronal anneal, the optical spectrum was initially recorded at 77 K; then an immersion heater was used to quickly warm the sample to the specified temperature which was maintained for ten minutes. The sample was then quenched to 77 K and an optical spectrum was recorded. Above ambient temperature, a small laboratory box furnace

(Model 51844, SB LINDBERG) capable of holding the sample at constant temperature up to 1300 K was used. After 10 minutes at temperature, the sample was removed and quenched on a brass block at 300 K. The optical spectrum was then recorded.

Irradiation procedure

Crystals of $RbCdF_3$ were electron-irradiated at 300 K or 77 K. The source of electrons was a Van de Graaff accelerator (1.7 MeV, 0.2 $\mu A/cm^2$) and the total dose received by each sample was approximately 10^7 rad (Si).[37] Figure 7 is a schematic drawing of a liquid-nitrogen cryostat of the type frequently used for irradiation experiments. The crystal is mounted on a copper holder attached to the liquid-nitrogen reservoir. Good thermal contact must be made between the sample and the holder. Irradiations were carried out through the cryostat's aluminum window with the sample located 10 cm from the Van de Graaff's aluminum foil window.

In addition, sample heating during the irradiation was avoided by irradiating for five minutes intervals separated by two minutes with no irradiation.

Data calibration

The emission spectra were corrected by using a General

lElectric QL-157 quartz-iodine standard lamp, whose characteristics are traceable to the National Bureau of Standards.

A Pyroelectric Radiometer PR200 from Molectron Corporation was placed at the sample position and used to correct the excitation spectra. Pyroelectric Detector Model PR-20 was adopted for intensity readings on a calibrated scale from 250 nm to 900 nm. Figures 8 and 9 show the appropriate calibration data in intensity versus wavenumber for excitation and emission spectra, respectively, from this experiment. Below 250 nm the intensity of the xenon lamp is too weak to be useful.

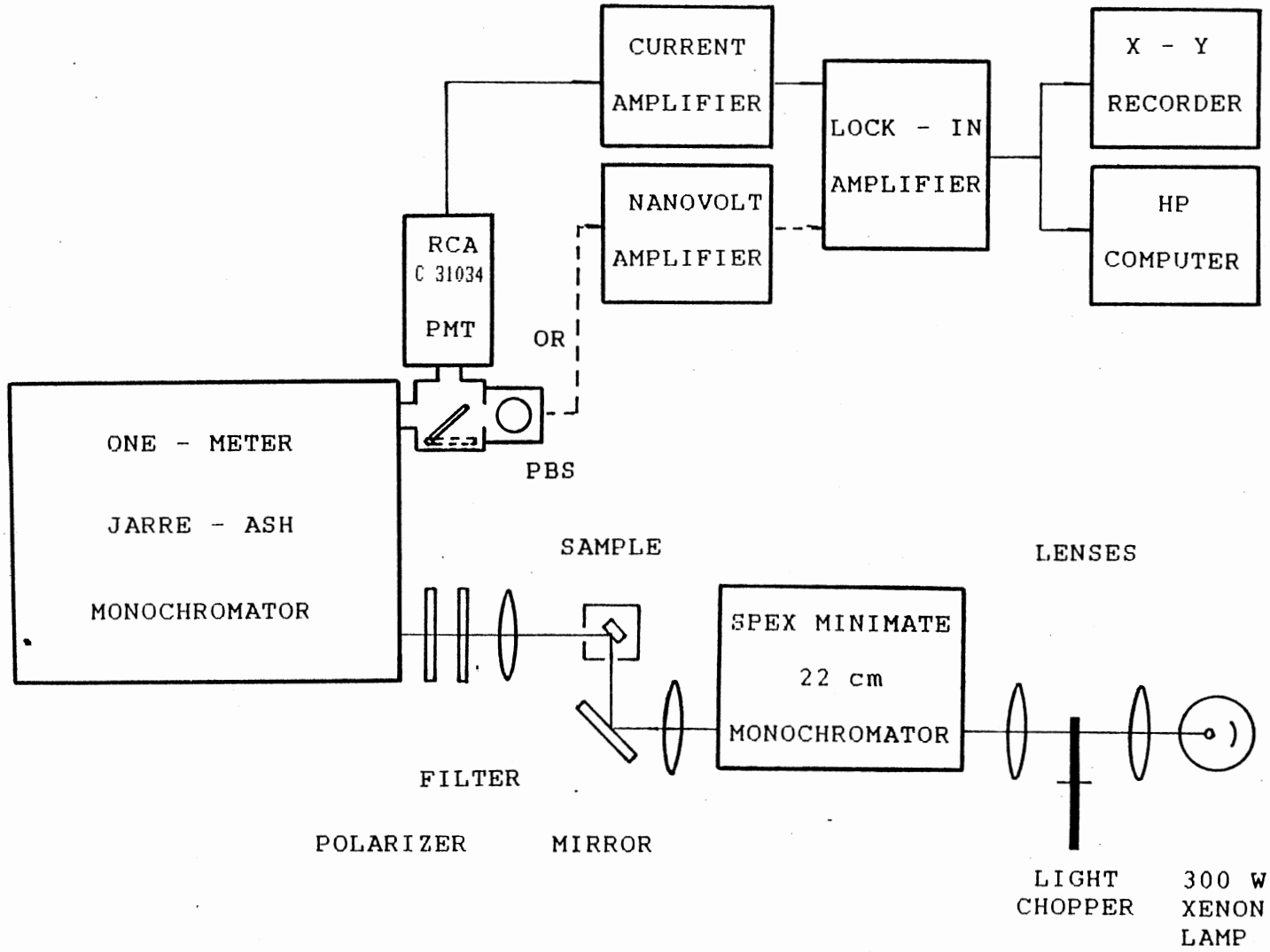

Figure 6. Block diagram of the experimental system for visible and infrared luminescence

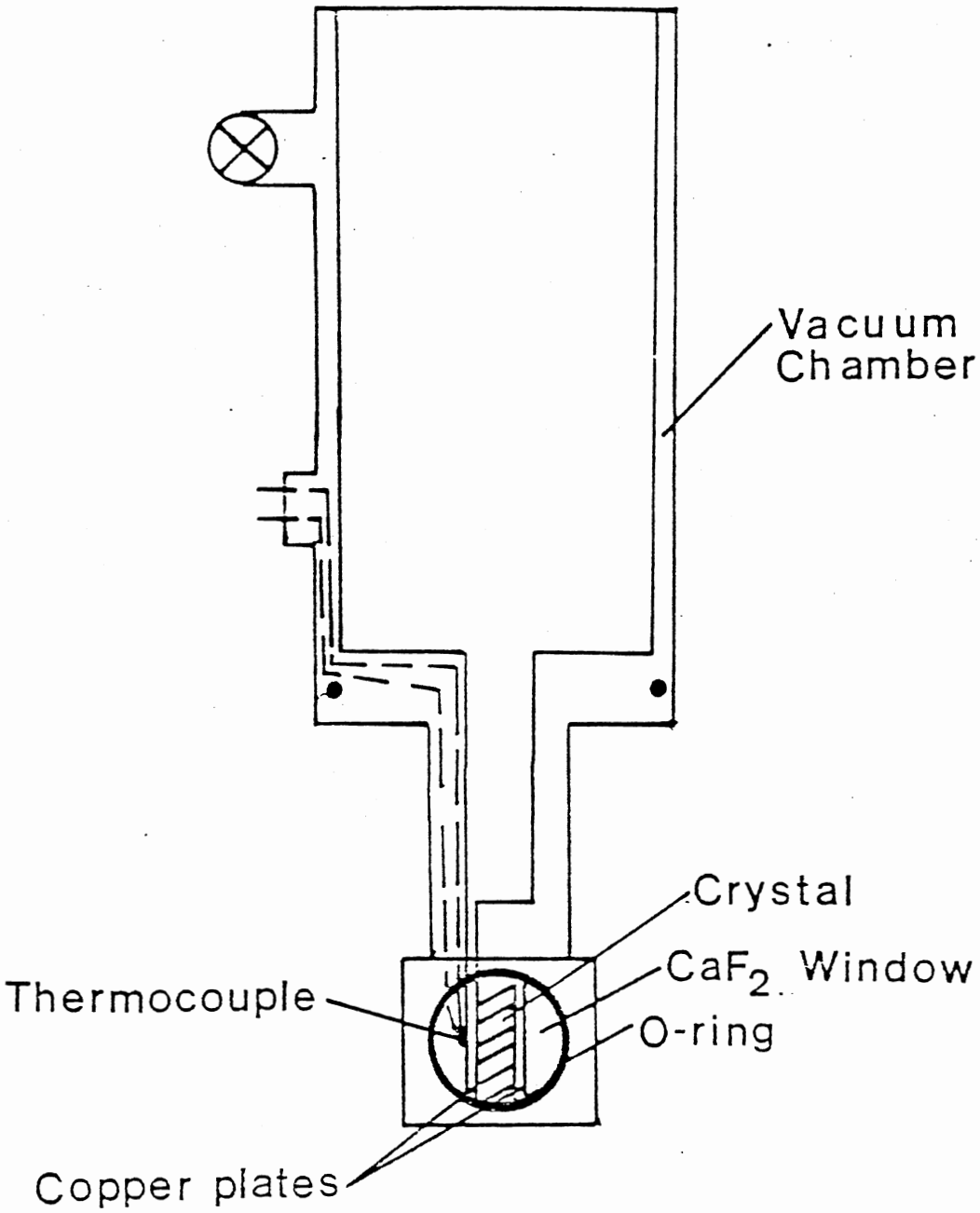

Figure 7. Schematic diagram of the cryostat used for low temperature irradiation and optical measurement

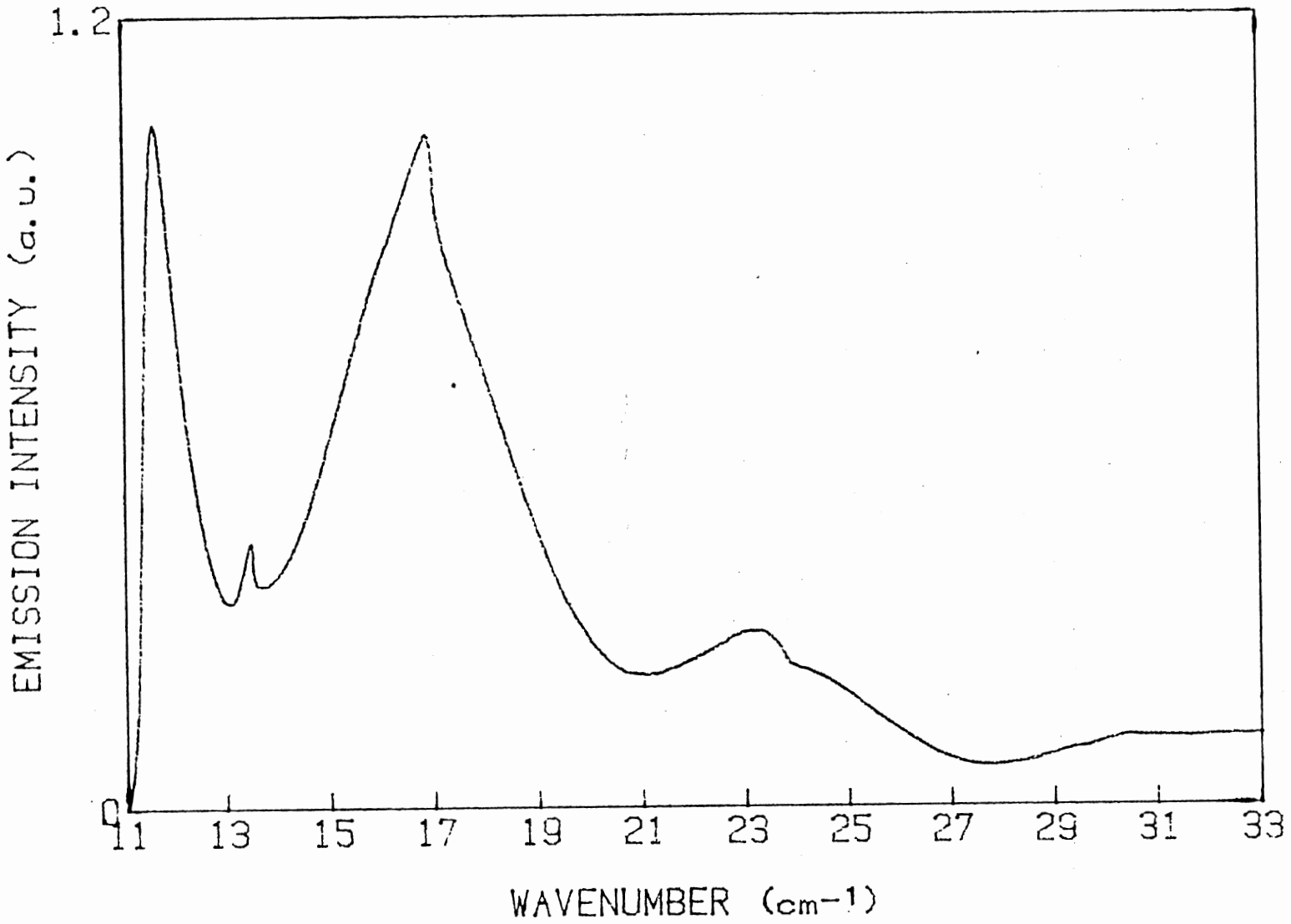

Figure 8. Calibration data for emission spectra

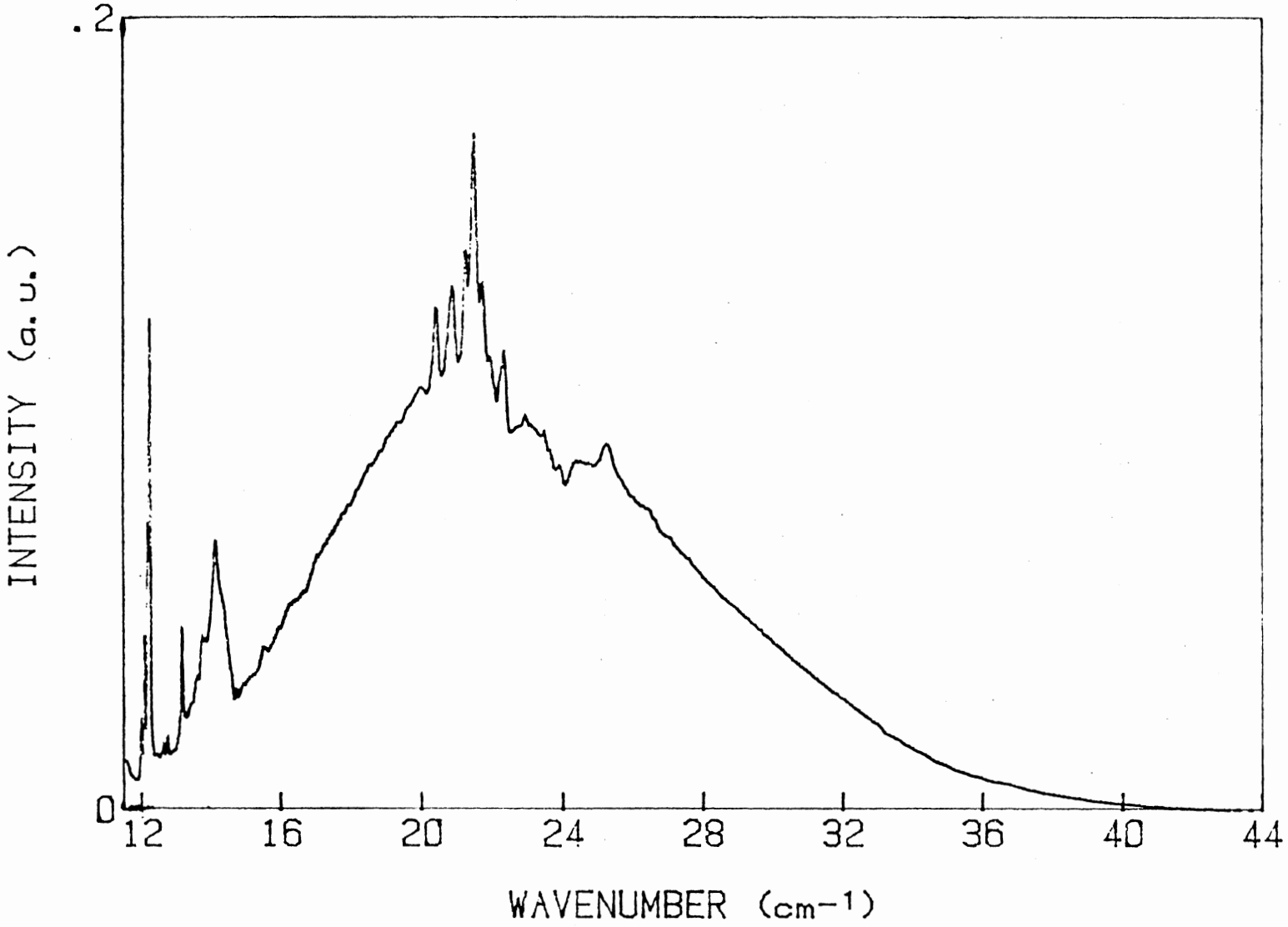

Figure 9. Calibration data for excitation spectra

CHAPTER III

RADIATION DAMAGE IN PURE $RbCdF_3$ AND $RbCdF_3:Mn^{2+}$

Experimental results

The absorption spectra of $RbCdF_3$ crystals after irradiation at either liquid nitrogen temperature or room temperature are rather complex. Figure 10(a) depicts a typical absorption spectrum of pure $RbCdF_3$ measured after an electron irradiation at 77 K to a dose of about 0.5×10^{14} MeV/cm^3. The radiation-induced absorption band is clearly a combination of several broad bands corresponding to different defect centers. The apparent peak positions are at 286 nm, 316 nm, and 365 nm. The 365 nm band saturates rapidly with irradiation. Figure 10(b) illustrates the absorption for a Mn^{2+} doped sample irradiated to a dose of 0.5×10^{14} MeV/cm^3. It is apparent that the same bands appear in the absorption spectrum for this case as well. Fiqure 11(a) is a plot of the absorption spectrum for pure $RbCdF_3$ irradiated at 77 K to a very high dose of 138×10^{14} MeV/cm^3. The lower portion of Fiqure 11 is a similar portrayal for $RbCdF_3:Mn^{2+}$. Notice that in the case of the pure crystal, an extra band appears in addition to the 286 nm, 316 nm, and 365 nm bands. In the case of the heavily

doped sample only the 286 nm band appears. This is not unrealistic. For example, as mentioned earlier, the absorption due to $X_2(V_k)$ centers saturates rapidly at low doses. In a doped crystal, in particular, the X_2 band saturates and the interstitials are trapped at impurities so the H center band will not be present. Only the band associated with F-centers will appear at high doses.

In order to identify the various bands, a series of experiments was undertaken. First, the thermal stability of the defects was investigated. For example, samples irradiated at a low temperature were warmed to higher temperatures. The $X_2(V_k)$ centers tend to anneal at lower temperatures or can be bleached optically. In pure materials, the H-centers and the F-centers will anneal simultaneously and also will grow together with irradiation dose. Thermal annealing and bleaching experiments on the samples whose data are shown in Fiqures 10 and 11 were made. It was possible by comparing heavily irradiated doped material with lightly irradiated pure material to determine that the three dominant bands were as shown in the figures. The peak energy and halfwidth of each band is listed in Table 1. These three major bands can be used to fit all absorption spectra at various radiation doses or annealing stages for all of the samples. For example, Figure 12 illustrates an intermediate irradiation dose for an Mn^{2+} doped sample. Notice that the appropriate absorption

coefficients for each of the three major bands allow a fit to these data as well as to those of Figure 10 and 11.

Once the major bands have been determined, it is possible to chart a radiation growth curve. Figure 13 is a plot of absorption coefficient at the peak of the various bands, as noted on the figure, versus irradiation dose for pure $RbCdF_3$. Note the 365 nm band which we believe is the $X_2^-(V_k)$ center saturated very rapidly whereas the bands due to F-centers at 286 nm and H-centers at 316 nm continue to grow. This same growth is quite evident in Fiqure 14, which illustrates growth of centers in the doped material. It is also evident that the pure H-centers in this material actually decay with irradiation dose. This is due to the H-centers being trapped at Mn^{2+} ions and the pure H-center absorption then disappears as this occurs.

The thermal annealing behavior for both pure and doped $RbCdF_3$ crystals are shown in Figures 15, 16, and 17. After an electron irradiation at 77 K , a sample was held for ten minutes at a specified temperature, then quenched to 77 K, where all the absorption spectra were taken. This process was repeated several times for different annealing temperatures. The annealing curves for the pure sample are demonstrated in Figure 15 and show the range of thermal stability of both X_2^- centers, H- and F-centers. It is evident that the major bands anneal simultaneously. This is depicted more clearly in a plot of the 286 nm absorption due to F-centers versus the 316 nm absorption due to H-centers

for both irradiation growth and thermal annealing treatments in Fiqure 16. Notice that these two types of centers grow in and out together. This indicates a mutual relationship. Namely, that as the interstitials become mobile, they do move to annihilate F-centers. When Mn^{2+} doped $RbCdF_3$ crystals are electron irradiated at 77 K with a heavy dose, stable F-center defects are formed. The absorption band due to F-centers at 77 K is at 286 nm (34965 cm^{-1}) with halfwidth of 0.68 eV. At room temperature the band is at 296 nm (33784 cm^{-1}) with a halfwidth of 0.85 eV as shown in Figure 17. This illustrates the temperature dependence of the F-center since no other bands appear to be present in this heavily irradiated material. Such data allow us to portray a thermal annealing curve for this material as presented in Figure 18. Since the annealing data for both 77 K irradiation and 300 K irradiation agree in the Mn^{2+} doped samples this indicates the interstials are trapped at Mn^{2+} ions. The marked difference radiation in the annealing of the pure $RbCdF_3$, F centers also suggests interstitial trapping in the doped material. The inset illustrates that for room temperature electron irradiation saturation of the F-center growth does occur at high doses. It is also important to note that as self-trapped excitons recombine through the migration of V_k-centers, F- and H-centers can be produced. This has been observed previously, and is quite evident in Figure 19 for a lightly irradiated Mn^{2+}-doped sample. With annealing there is a loss of V_k-centers in the

low energy region of the spectrum and a definite growth of H- and F-centers in this material. The inset shows that this growth occurs at the same temperature as V_k annihilation. This electron-hole recombination occurs at 260 K for pure $RbCdF_3$ and at 160 K for Mn^{2+}-doped sample.

Figure 20 shows the emission spectra excited at 300 nm after electron irradiation for $RbCdF_3$ crystals. The emission band at 450 nm is similar to those ascribed to the recombination of H- and F-centers in other materials.[38]

TABLE I

PEAK ENERGIES AND HALFWIDTHS OF
F-, H- AND V_k- CENTERS IN $RbCdF_3$

	PEAK ENERGY E (cm^{-1})	HALFWIDTH W (eV)
F BAND (77 K)	34965	0.68
(300K)	33784	0.84
H BAND (77 K)	31646	0.45
V_k BAND (77 K)	27397	0.57

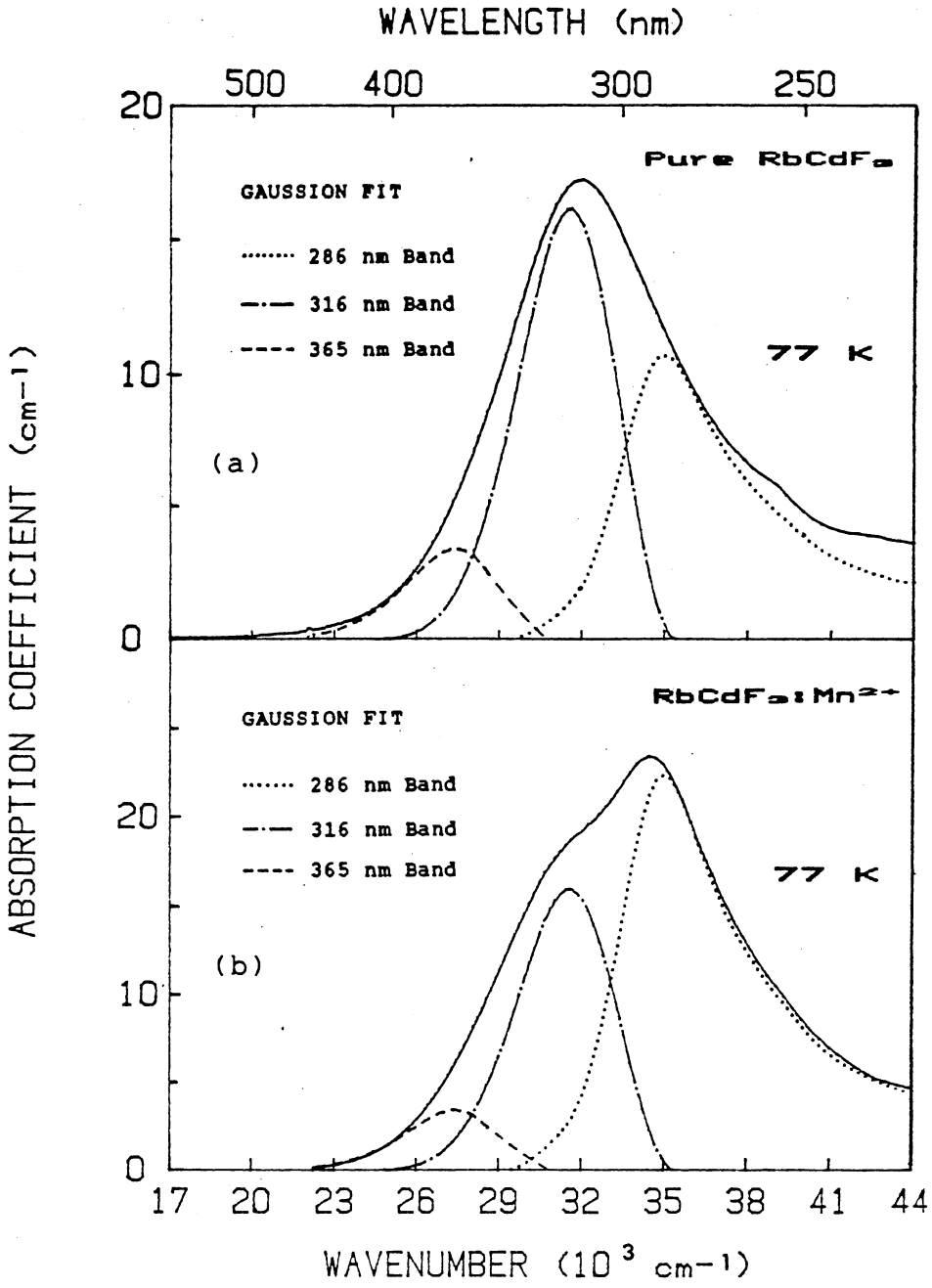

Fig. 10. Absorption spectra of (a) pure $RbCdF_3$ and (b) $RbCdF_3:Mn^{2+}$, electron irradiated at 77K to a dose of 0.5 X 10^{14} MeV/cm^3 and Gaussian fits

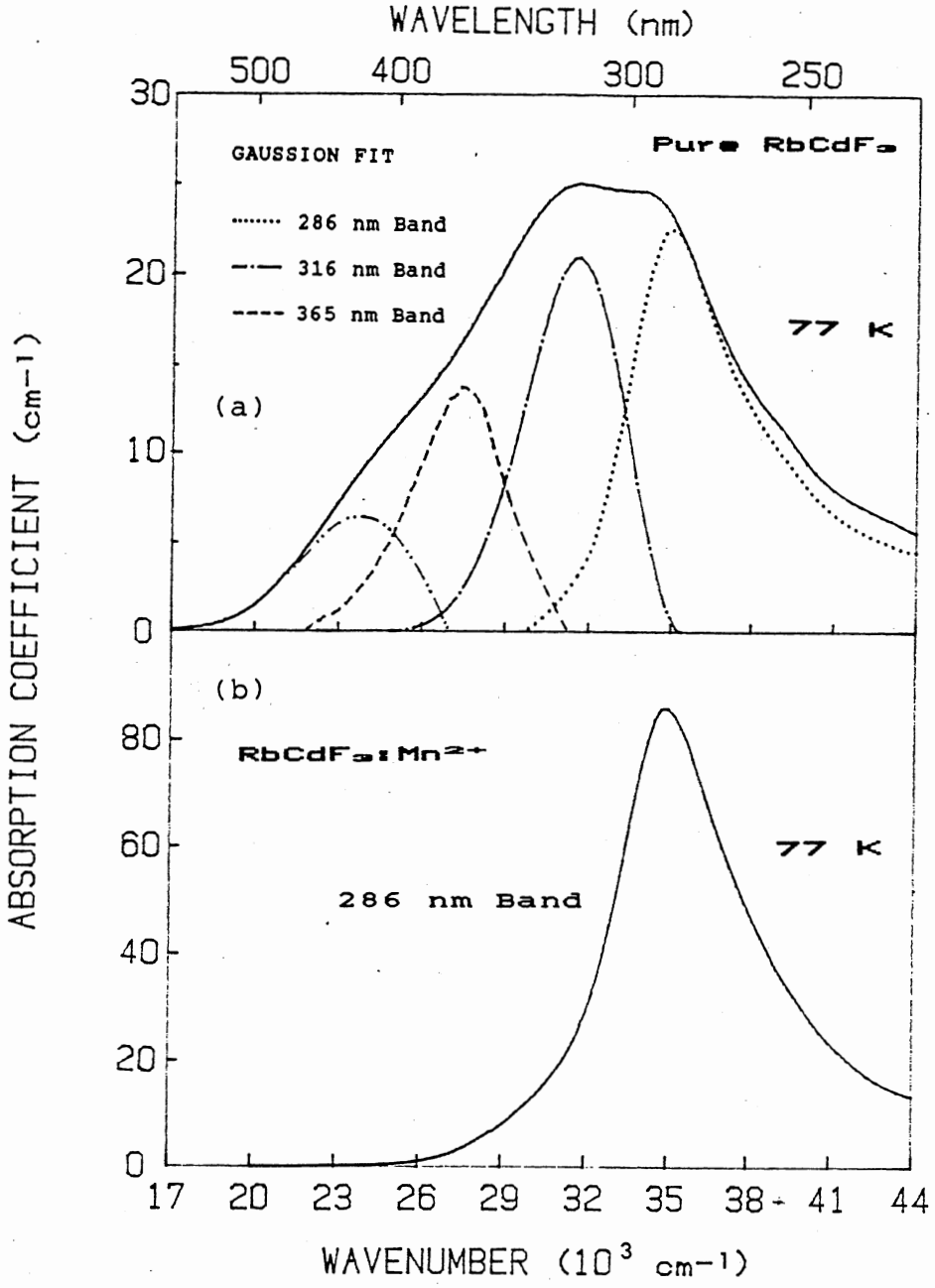

Fig. 11. Absorption spectra of (a) pure $RbCdF_3$ and (b) $RbCdF_3:Mn^{2+}$, electron irradiated at 77 k to a dose of 138 X 10^{14} MeV/cm^3 and Gaussion fits

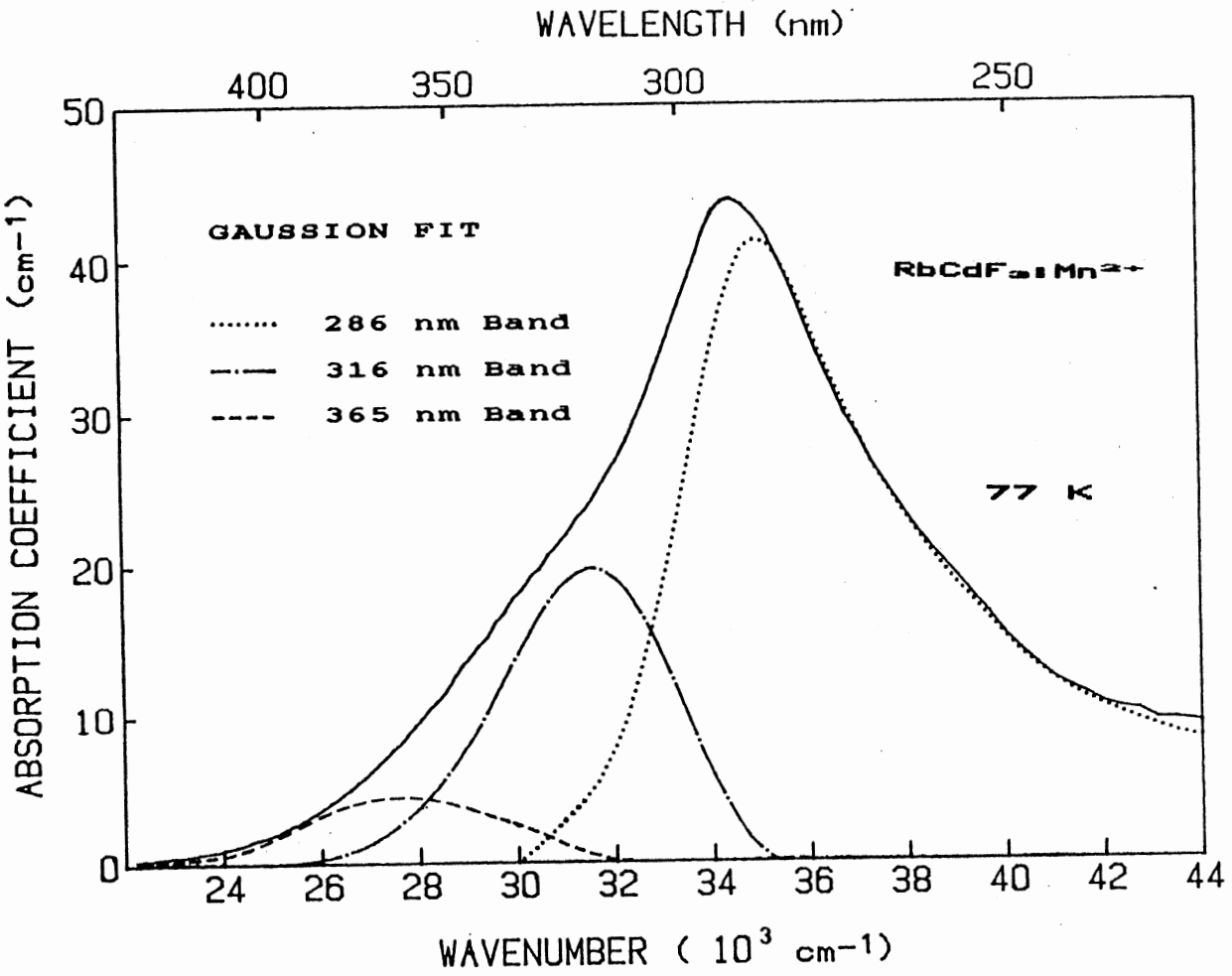

Fig. 12. Absorption spectra of $RbCdF_3:Mn^{2+}$ irradiated at 77K to a dose of 50 X 10^{14} MeV/cm^3 and Gaussion fits

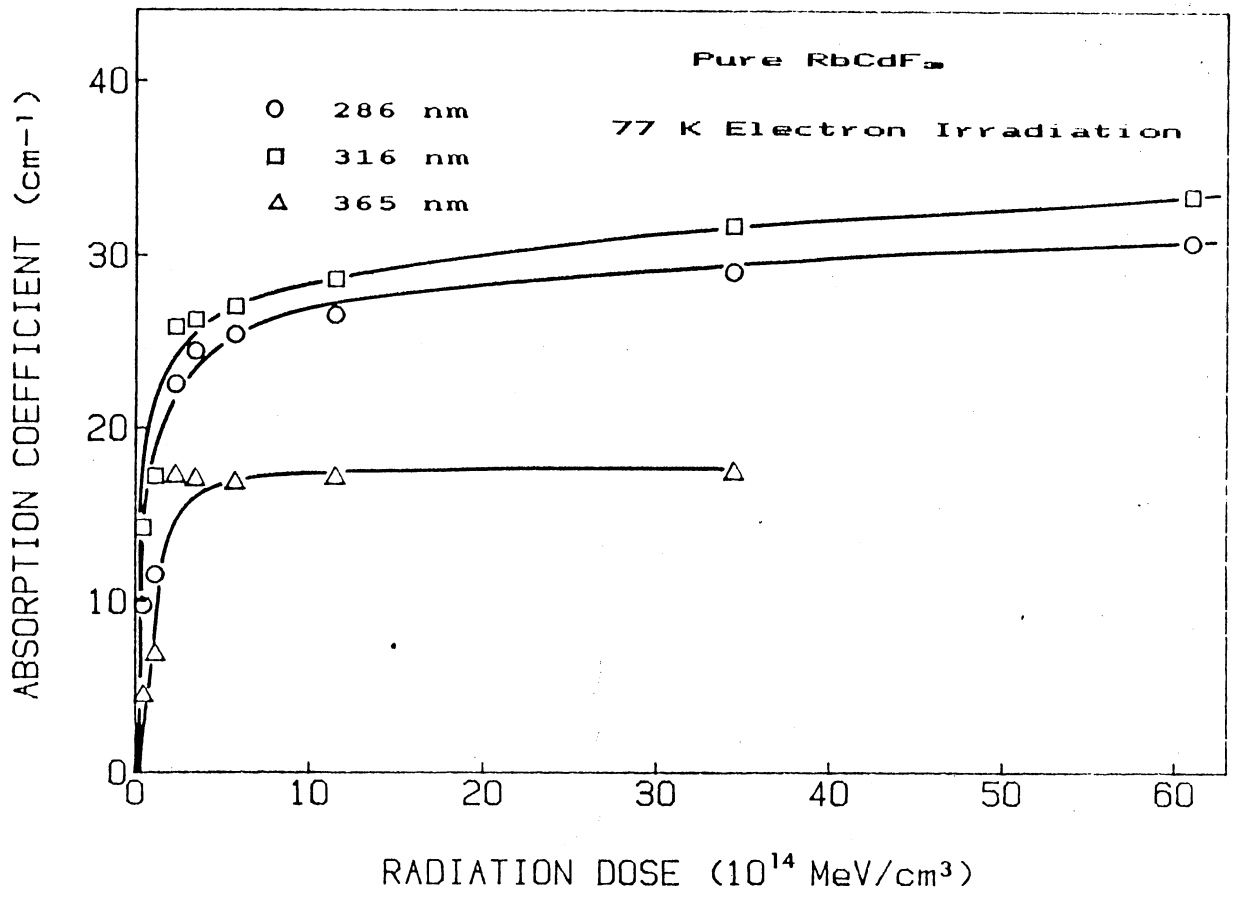

Figure 13. Growth curves of 286 nm, 316 nm and 365 nm bands at 77 K for 77 K irradiated pure $RbCdF_3$

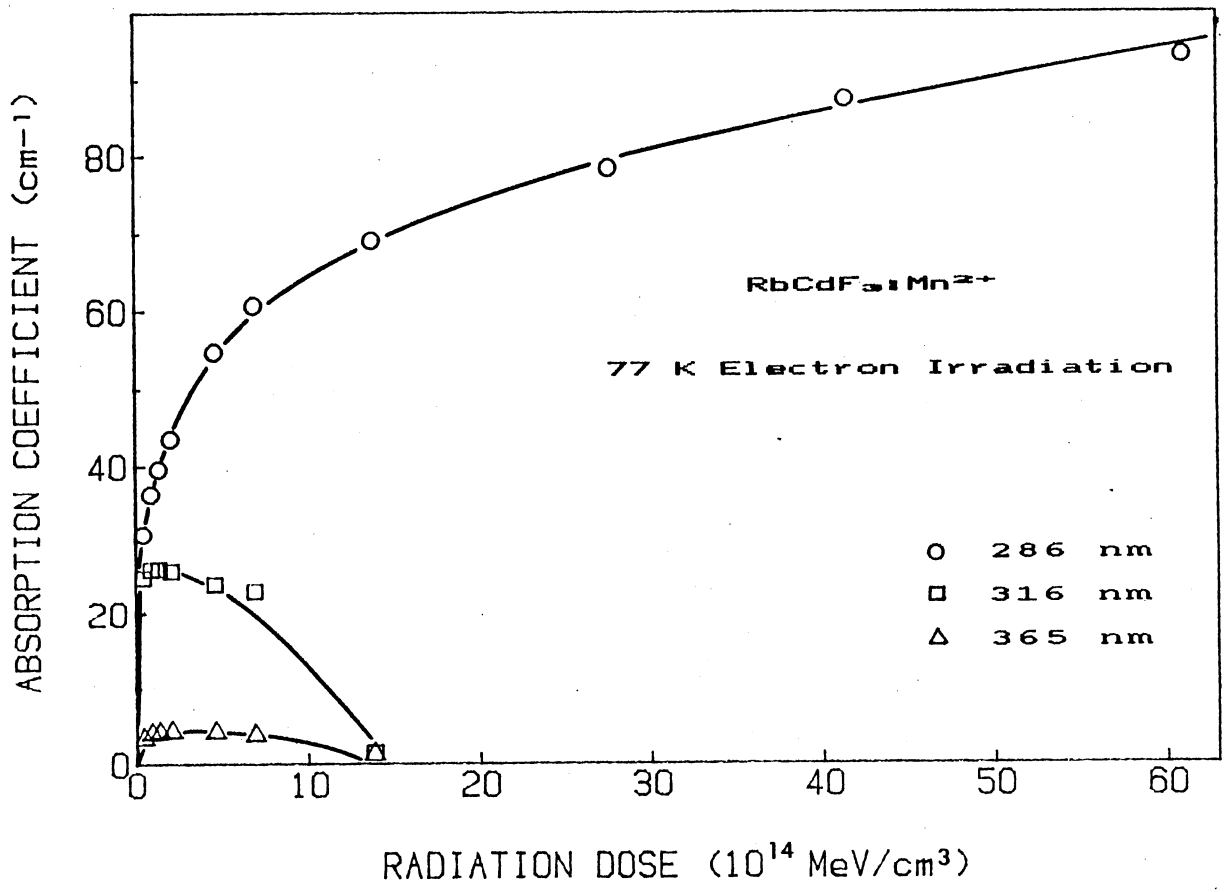

Figure 14. Growth curves of 286 nm, 316 nm and 365 nm bands at 77 k for 77 k irradiated $RbCdF_3:Mn^{2+}$

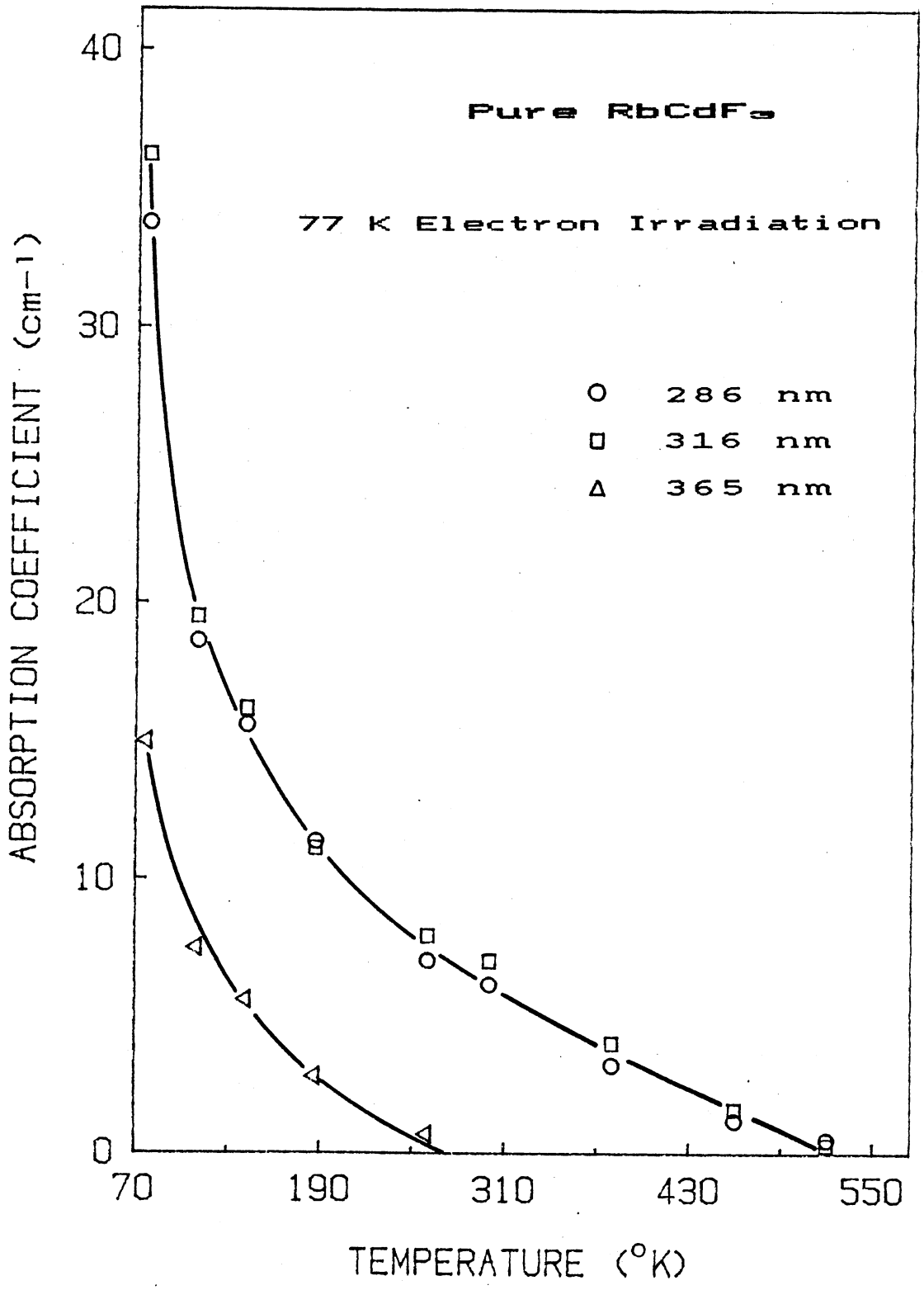

Figure 15. Annealing curves of 286 nm, 316 nm and 365 nm bands for pure $RbCdF_3$ at 77 K

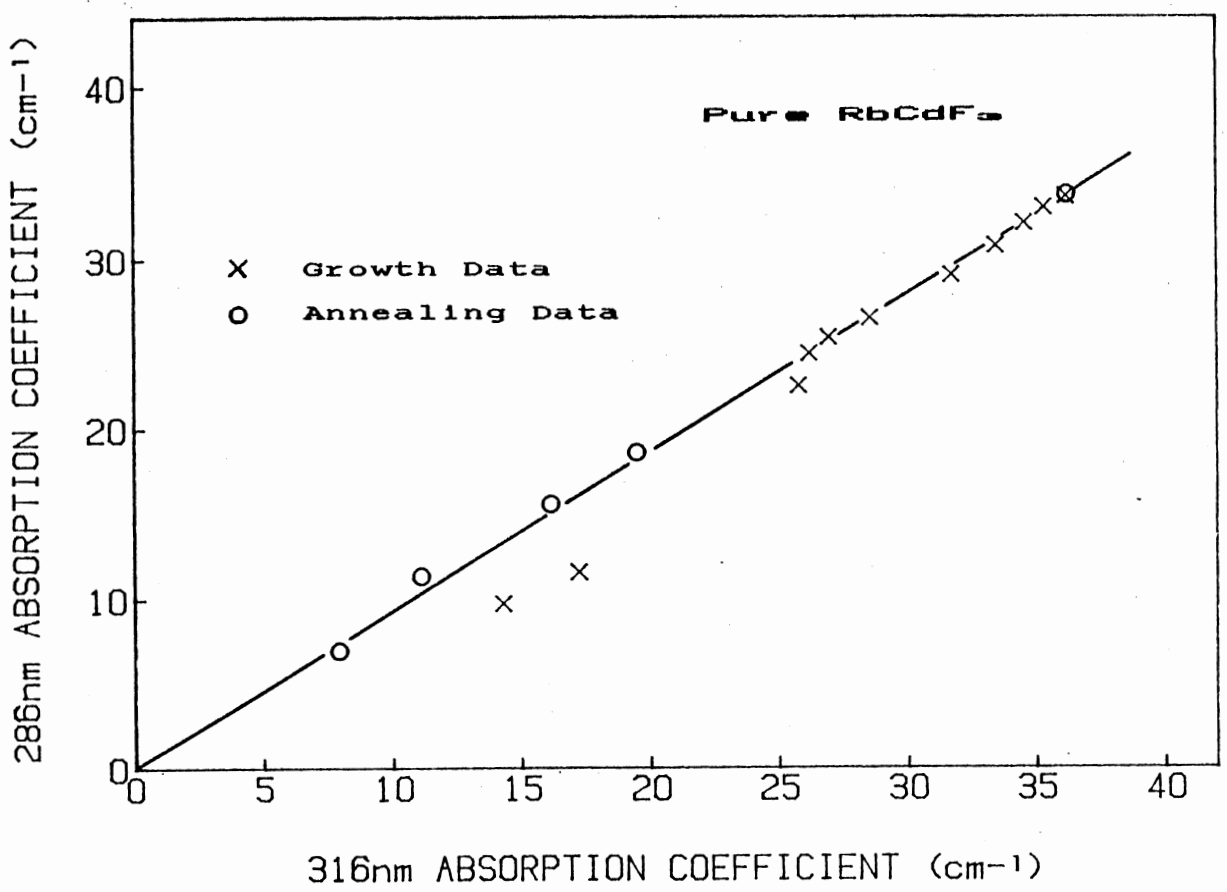

Fig. 16. A plot of absorption coefficient of 316 nm vs. that of 286 nm from both irradiation growth data(cross) and thermal annealing data (circle) in pure $RbCdF_3$

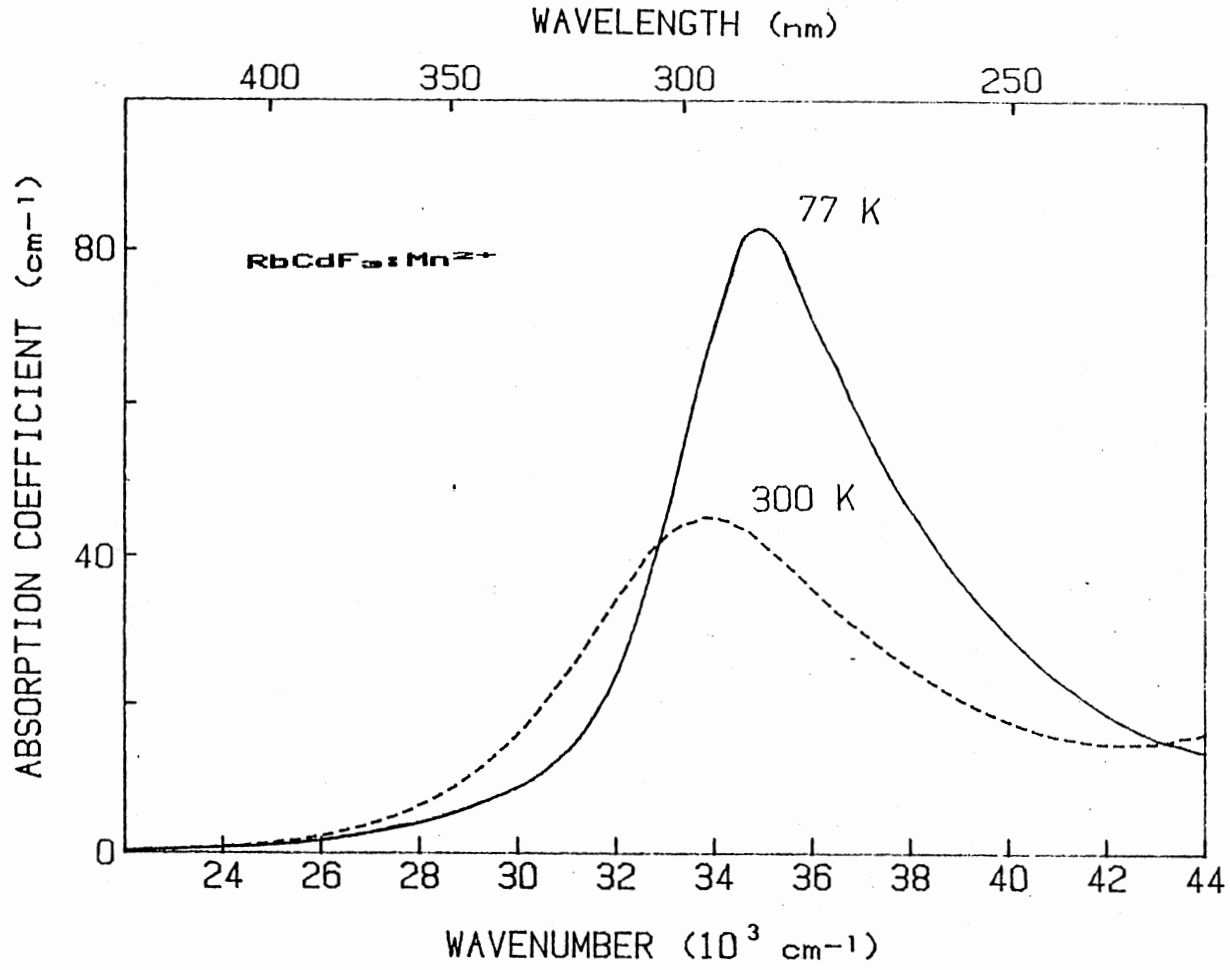

Figure 17. Temperature dependence of F-bands between 77 k and 300 k in $RbCdF_3:Mn^{2+}$

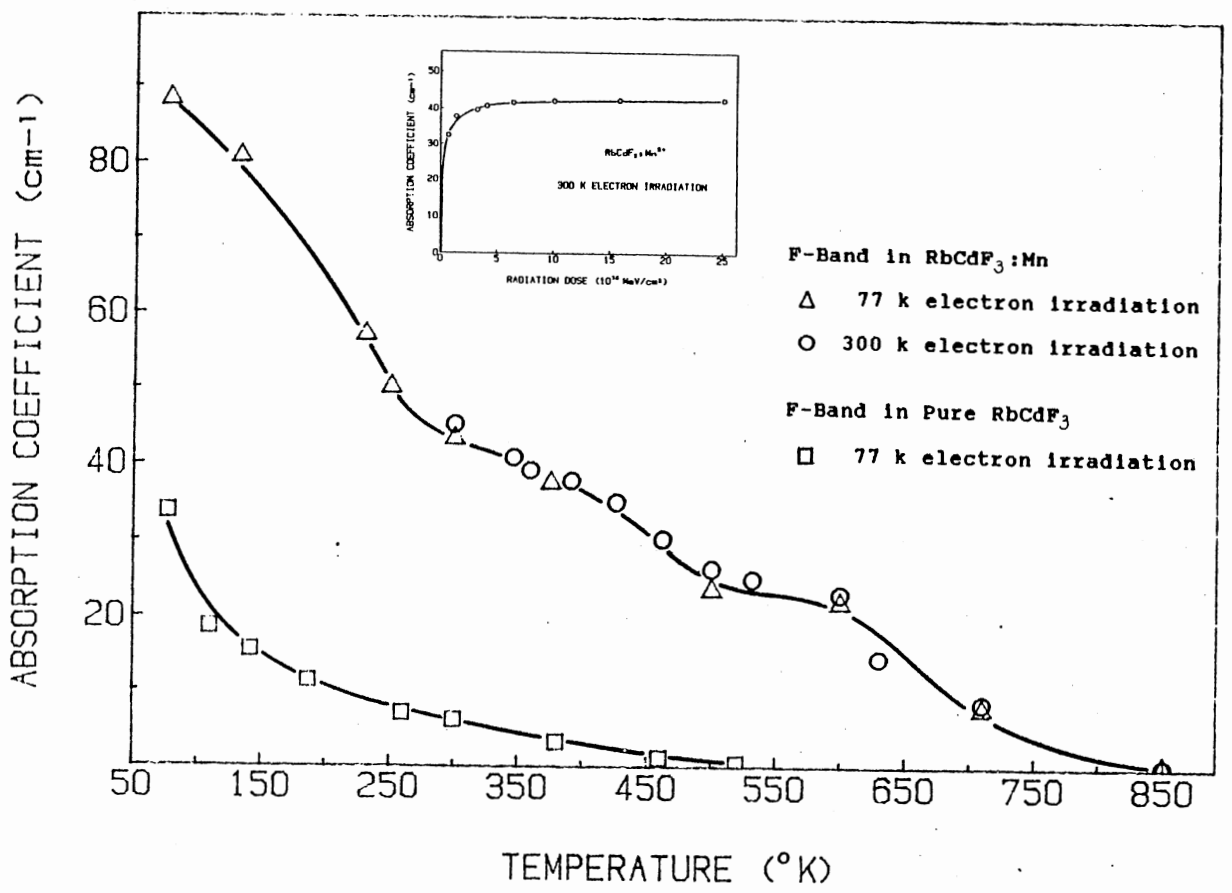

Fig. 18. Thermal annealing curves of F-centers for both pure $RbCdF_3$ and $RbCdF_3$:Mn^{2+}. The inset is growth curve of F band irradiated at 300 k for Mn-doped $RbCdF_3$

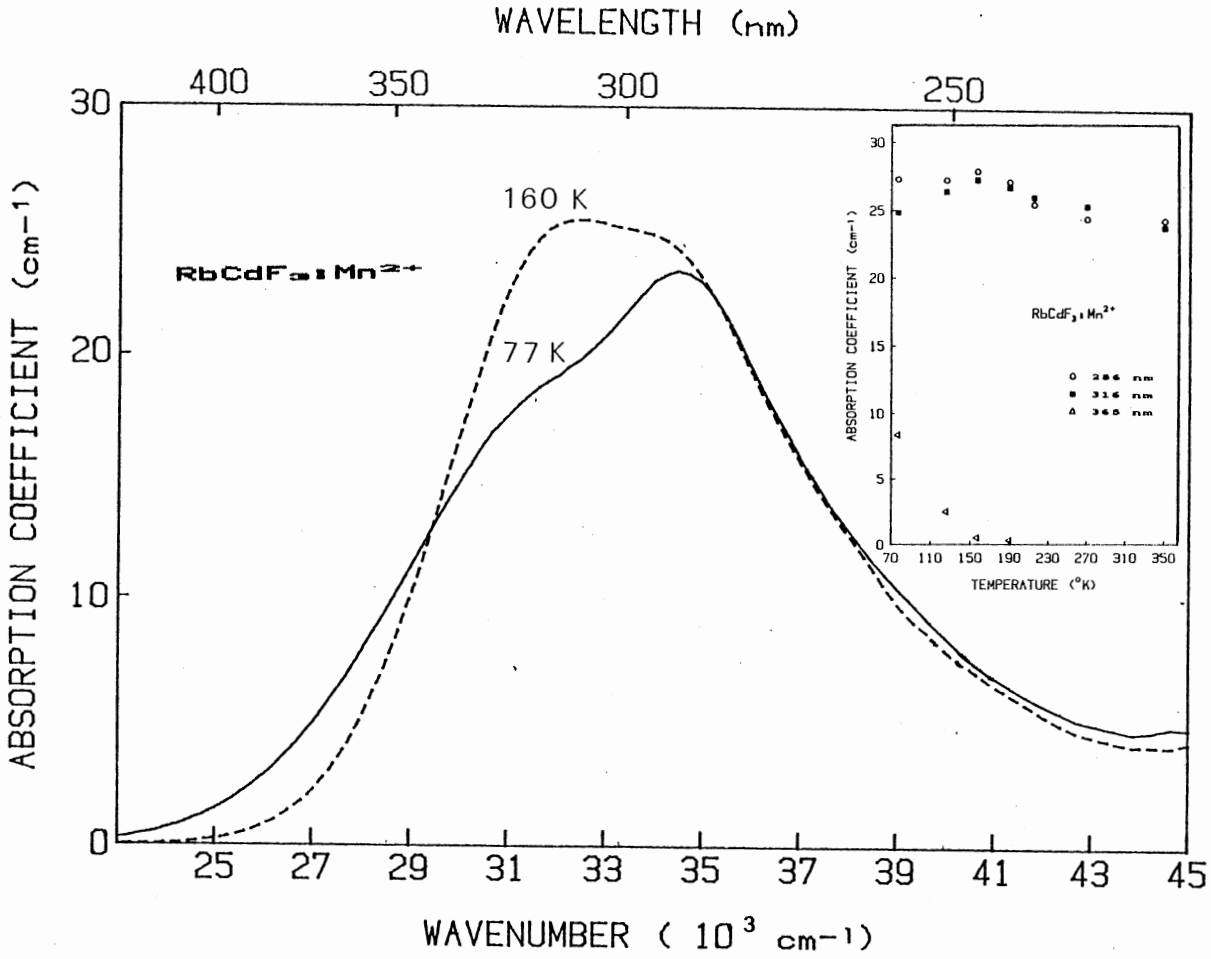

Fig. 19. Absorption spectra of $RbCdF_3 : Mn^{2+}$ for thermal annealing to 160K after electron irradiation at 77K with low dose. The inset shows the annealing behavior of 286nm, 316nm and 365 nm bands in $RbCdF_3:Mn^{2+}$ for low dose irradiation at 77 k

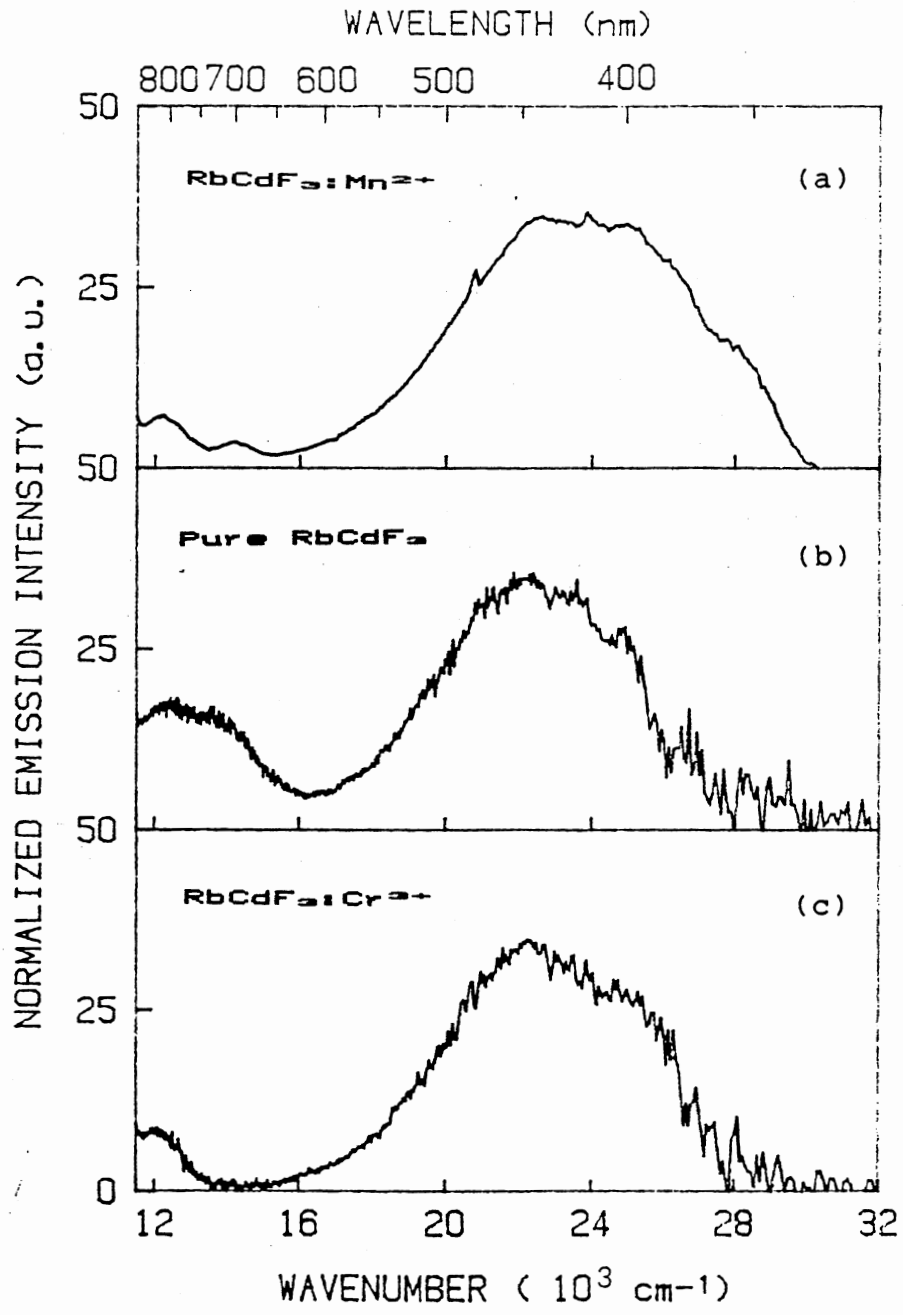

Fig. 20. Emission spectra of (a) $RbCdF_3:Mn^{2+}$, (b) pure $RbCdF_3$ and (c) $RbCdF_3:Cr^{3+}$, excited at 300 nm after electron irradiation

Discussion

The present experimental evidence indicates that close F-H pairs are introduced into pure $RbCdF_3$ crystals by electron irradiation at 77 K. The generation of Frenkel pairs is triggered by the formation of $X_2^-(V_k)$ centers and the reaction, $X_2^- + e \longrightarrow F + H$. That is in agreement with previous work.[18-23]

From the research of Williams et al,[30] the peak energies of the stable bands of F-, H-, and V_k- centers can be expressed as functions of crystal parameters in terms of the average distance from fluorine ions to the nearest-neighbor cations. This significant correlation for four fluoride crystals, MgF_2, CaF_2, SrF_2, and BaF_2, are illustrated in Fiqure 5 by Williams et al. In $RbCdF_3$, the nearest-neighbors to fluorine ions are 2.2 Å from Cd^{2+} ions and 3.11 Å from Rb^+ ions, respectively. From Figure 5 the peak energies of stable bands in $RbCdF_3$ can be extrapolated. It is expected that the F, H and V_k bands in $RbCdF_3$ will occur at 4.2 eV, 4.1 eV, and 3.9 eV, respectively. Compared with the measured energies illustrated in Figure 5, as 4.3 eV, 3.92 eV and 3.4 eV for F, H and V_k bands, respectively, it is clearly seen from this figure that the present experimental results for F- and H-centers agree with this prediction very well. Since radiation induced F-, H- and

V_k-centers in fluorine crystals, such as CaF_2, MgF_2, $RbMgF_3$, $KMgF_3$ and $RbCaF_3$, have already been experimentally studied by numerous researchers,[39-44] it is worthwhile to explore the basic mechanisms by comparing the relevent data from the present study with those previous results. The absorption peak energies and halfwidths of the color centers in various crystals are listed in Table II. It is of interest to note based on these data that the energy is strongly crystal-dependent for the F-band but not for the H- and V_k- bands. In Fig.21 the energy of the F-band is plotted against the nearest-neighbor distance of the crystals to show the dependence. This F-band energy-crystal relationship can be expressed as follows by using the least-square fitting technique:

$E = 16.958 * R_{nn}^{-1.7728}$ For alkali halide crystals

$E = 57.147 * R_{nn}^{-3.3317}$ For alkali earth halide crystals

$E = 6.54 * R_{nn}^{-0.5074}$ For perovskite crystals

Where R_{nn} is the nearest-neighbor distance from fluorine to cation in Angstrom units.

Figure 22 shows the correlation of the energies of H- and V_k-bands vs. nearest-neighbor distances of alkali halide, alkaline-earth halide, and perovskite crystals. No significant influence of crystal structures on the energy levels was found for both the H- and the V_k-centers.

The comparative data shown in Figures 13 and 14 suggests that the presence of divalent manganese ions in $RbCdF_3$ crystals leads to a greater concentration on F-centers. Also it is evident that the growth of H-bands is reduced with increasing irradiation dose and eventually vanishes in the Mn^{2+}-doped specimen. In order to analyze the probability of interstitial trapping by Mn^{2+} impurities in this material, the concentration of Frenkel pairs produced in pure $RbCdF_3$ crystal must be evaluated. Since appreciable F aggregation does not occur at this temperature, the number of F-centers is an indication of the number of Frenkel pairs. Assume the concentration of the F- and H-centers to be the same, then the number of Frenkel pairs can be obtained from Smakula's Equation,[49,50]

$$f * N = 7.3 * 10^{15} \alpha_m W \quad (cm^{-3})$$

where f -- the oscillator strength

N -- the concentration

α_m -- the maximum absoption coefficient

W -- the halfwidth of the band

The oscillator strength of the F-center is assumed to be 0.5 for Gaussian form. The number of F-centers in a pure crystal at a radiation dose of 4×10^{16} MeV/cm^3 is calculated to be about 2.7×10^{17} cm^{-3} from an $\alpha = 30$ cm^{-1}. The distance between F-centers corresponds to 34 lattice sites. The Mn^{2+} concentration of 1.76×10^{20} cm^{-3} corresponds to four lattice distances between Mn^{2+} ions.

The number of stable F centers in $RbCdF_3$: Mn^{2+} at saturation is 8 x 10^{17} cm^{-3}. This suggests that the enhancement of stable F-centers is due to H-centers trapped at Mn^{2+} ions. In view of the hypothesis of N. Itoh,[51-53] the interstitial trapping by impurities occurs if the displacement of halogens takes place within a certain volume around an impurity. The effective radius of the elastic interaction between the impurities and interstitials is to be 10 lattice distances. His suggestion does not contradict the present one.

In Figure 18, the annealing data of F-centers indicate that there is a difference of thermal annealing characteristics between pure and Mn^{2+}-doped $RbCdF_3$ crystals. Radiation-induced defects in doped samples anneal at a much higher temperature than in pure specimens. In pure $RbCdF_3$, the annealing can be expressed in terms of an exponential function of temperature. This suggests that when the temperature rises, interstitial motion occurs. The experimental results that F- and H-centers are produced and annealed together as shown in Fiqure 15 lend support to the above explanation.

For heavily irradiated $RbCdF_3$:Mn^{2+}, the F-center annealing curve shows the recombination annealing stages at the temperature ranges from 50 K to 250 K and 600 K to 850 K, respectively (Figure 18). The initial drop in absorption coefficient due to F-centers is about 50 % at 250 K. This is probably due to the release of interstitial,

trapped by Mn^{2+} ions during electron irradiation. At temperatures above 550 K, F-centers may become mobile and form F-aggregate centers or annihilate interstitial clusters. Our experiments at 300 K did not reveal any F-aggregate centers in this material. If F-centers were mobile at 300 K, various complexes of $F\text{-}Mn^{2+}$, or F_2 (M) centers would be expected. Based on limited studies carried out with this material, we suggest that F-centers are not mobile at room temperature in the 0.3 mol. % Mn^{2+} doped-$RbCdF_3$ crystal.

TABLE II

PEAK ENERGIES AND HALFWIDTHS OF
F-, H- AND V_k- CENTERS IN
CaF_2, MgF_2, $RbMgF_3$, $KMgF_3$, $RbCaF_3$ and $RbCdF_3$

	lattice constant (Å)	F		H		V_k	
		E (eV)	W (eV)	E (eV)	W (eV)	E (eV)	W (eV)
CaF_2	a=5.463	3.30	1.37	4.13	0.87	3.80	0.99
MgF_2	a=b= 4.623 c=3.052	4.77	0.60	4.13	----	----	----
$RbMgF_3$	a=5.83 c=14.27	4.20	0.92	4.13	0.20	3.76	0.95
$KMgF_3$	a=3.973	4.59	0.82	3.14	0.30	3.65	1.29
$RbCdF_3$	a=4.399	4.33	0.68	3.92	0.45	3.40	0.57
$RbCaF_3$	a=4.452	3.02	0.55	3.14	1.11	3.76	1.12

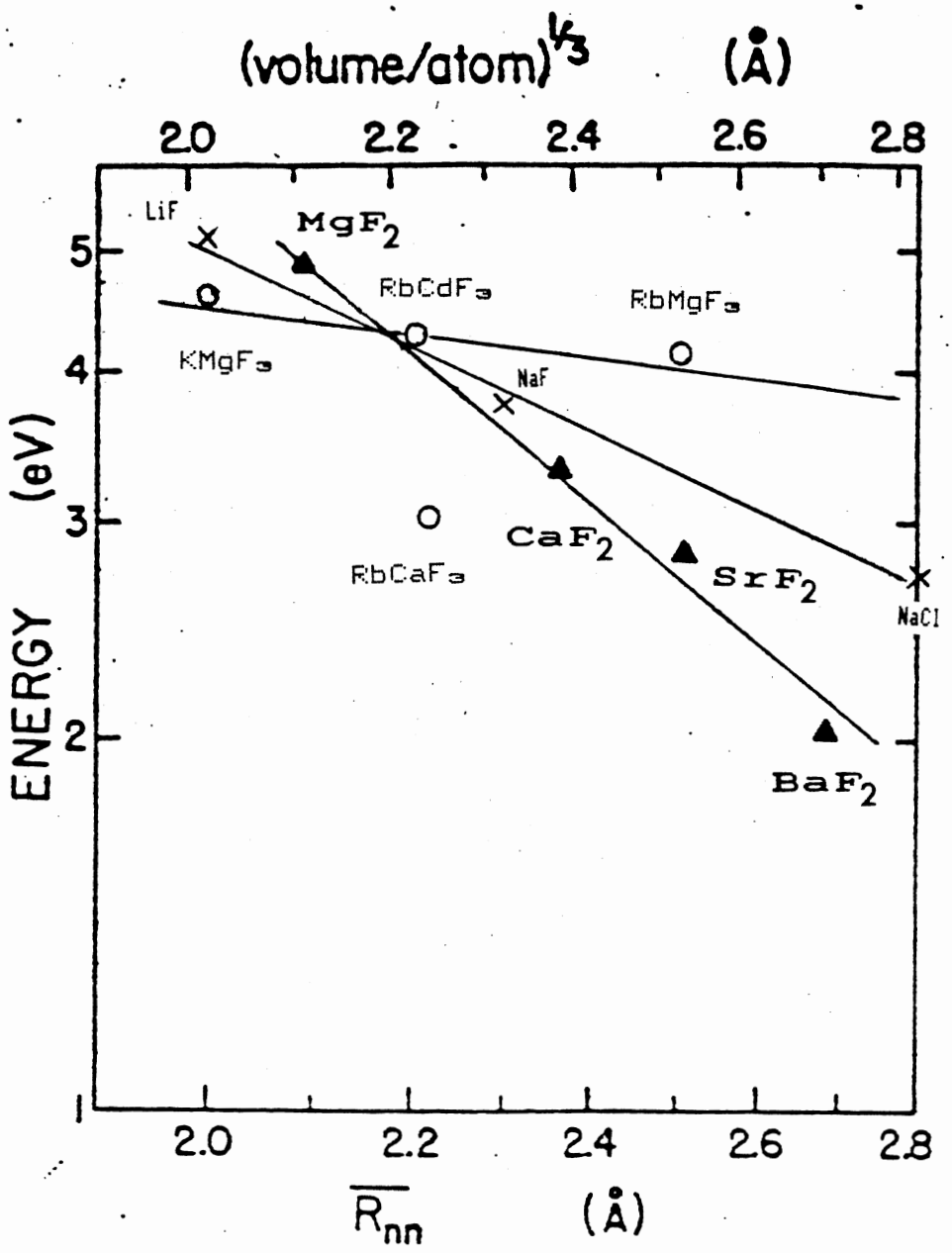

Figure 21. A plot of F-band absorption energies versus lattice parameter

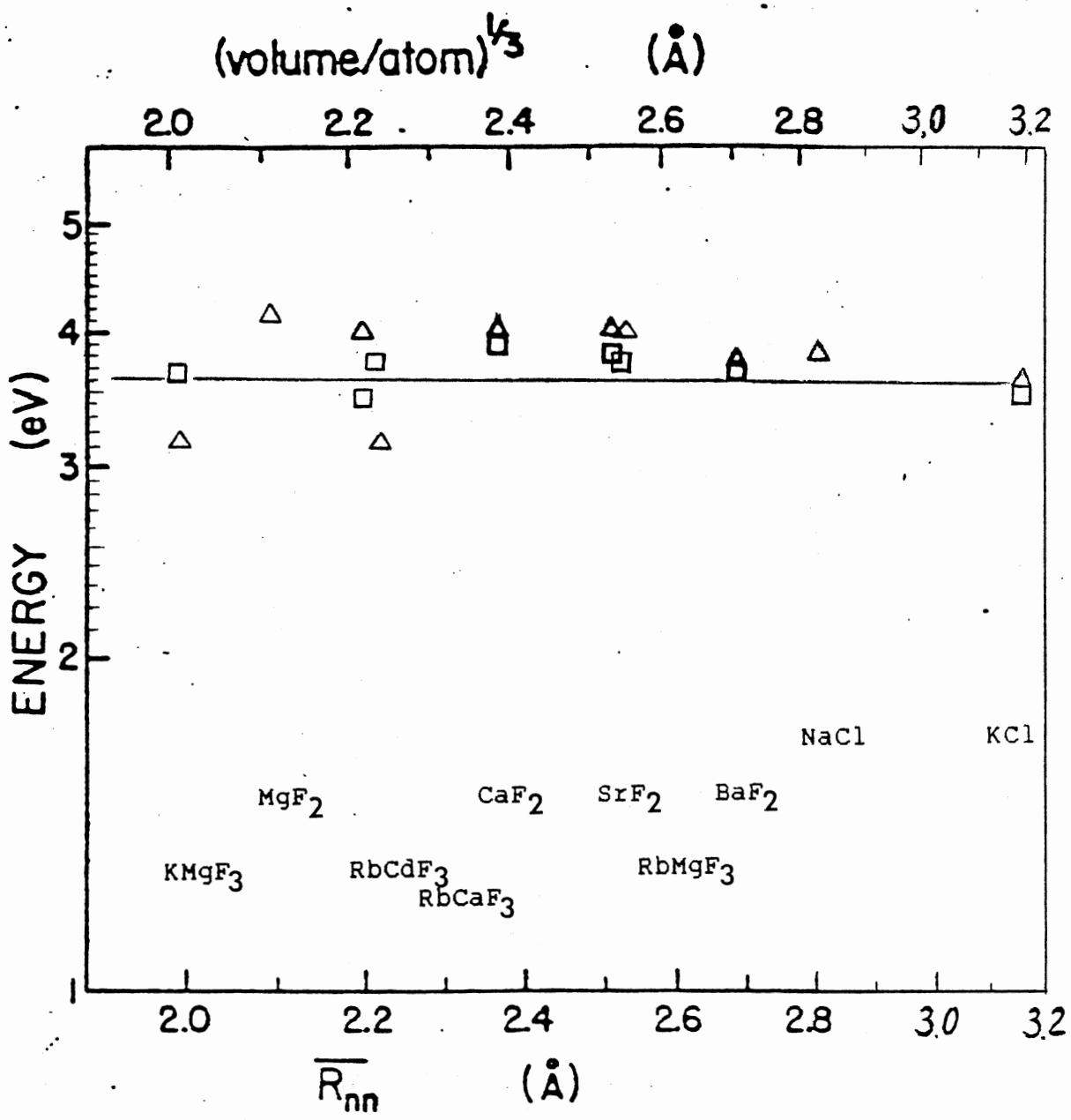

Figure 22. A plot of peak energies of absorption bands for H (□), V_k^- (△) centers against the lattice parameter

CHAPTER IV

OPTICAL PROPERTIES OF Mn^{2+} IONS IN $RbCdF_3$

The optical properties of Mn^{2+} have been extensively studied in a number of crystalline hosts.[54-59] In this chapter, the excitation spectra corresponding to the Mn^{2+} emission, and the temperature dependence of luminescence lifetimes of Mn^{2+} ion in $RbCdF_3$ have been investigated. The observed temperature dependence of Mn^{2+} emission in this material is discussed. Finally, limited data for Cr^{3+} in $RbCdF_3$ are shown for comparison.

Experimental results and discussion

Spectra

The manganese ion enters $RbCdF_3$ crystals as an impurity in a cation (Cd^{2+}) substitutional position due to the valence and size of the Mn^{2+}. Usually Mn^{2+} has a six-fold coordination environment (O_h symmetry) with a $3d^5$ electronic configuration in the ground state. The ground state of Mn^{2+} ions in $RbCdF_3$ is $^6A_{1g}$ (^6S). The transitions from the ground state to excited levels of the d^5 configuration in O_h symmetry are strongly parity and spin forbidden. Therefore, the oscillator strength of the absorption is quite small (10^{-7} --10^{-8}) and the lifetime of the ion in the

excited state is pretty long (1 -- 100 msec).[10] The optical absorption in our crystals is too weak to be observed between 200 nm and 2000 nm due to the low concentration of Mn^{2+}. In order to detect the transitions from the Mn^{2+} ground state $^6A_{1g}$ (^6S) to the excited levels within the d^5 configuration. The excitation spectra corresponding to the Mn^{2+} emission in $RbCdF_3$ consists of seven distinct bands centered at 19685 cm^{-1}, 23753 cm^{-1}, 25445 cm^{-1}, 28571 cm^{-1}, 30395 cm^{-1}, 35088 cm^{-1} and 41494cm^{-1} shown in Figure 23. The band at 25445 cm^{-1} is a double peak with splitting of 344 cm^{-1} (4 nm). These observed energies corresponding to the $^6T_{1g} \Longleftrightarrow {}^4T_{1g}{}^1$, ${}^4T_{2g}{}^1$, $^4A_{1g}$ ^4E_g, ${}^4T_{2g}{}^2$, ${}^4E_g{}^b$, ${}^4T_{1g}{}^2$ and $^4A_{2g}$ transitions, respectively. However, it is possible to use the Tanabe-Sugano diagram of O_h symmetry for Mn^{2+} to calculate a more precise assignment for the transitions. In Figure 24, the energy levels of the ground configuration of Mn^{2+} in cubic symmetry for transition energy versus crystal field [60] is shown. The energy has been normalized to the Racah parameter B. The crystal field parameters -- Dq, B, and C were determined from the data by the method of least squares. The observed energies corresponding to the $^6A_{1g} \Longleftrightarrow {}^4T_{1g}{}^1$, ${}^4T_{2g}{}^1$, $^4A_{1g}$, ${}^4T_{2g}{}^2$, and ${}^4E_g{}^b$ transitions were used in the fitting process. The results are listed in Table III. The normalized crystal fields, Dq in $RbCdF_3$, MgF_2 crystals and ZBLA glass are represented by the dashed, dash-dotted, and dotted vertical lines, respectively, in Figure 24, which

indicates the trend to the lower emission energy with increasing crystal field. The experimental data[61,62] of D_q listed in Table VI depicts the following series,

$$D_q(CaF_2) < D_q(CdF_2) < D_q(ZBLA) < D_q(RbCdF_3) < D_q(MgF_2)$$

It dose show the same order for corresponding emission energy, but not for ZBLA is probably due to the two different hosts.

Since the Mn^{2+} transitions from the ground state ($^6A_{1g}$) to excited states are both spin and symmetry forbidden, the oscillator strengths are quite low. However, it is possible to calculate[63] the oscillator strength from radiative lifetime for electron dipole transitions with the appropriate expression

$$f\ \tau = 1.51 * 10^{4} * (9 / n (n^2+2)^2) * X_o^2$$

where

f -- the oscillator strengths

τ -- the radiative lifetime in seconds

n -- the index of refraction

X_o -- the wavelength of the peak position in meter unit

If we assume radiative emission for the $^4T_{1g} \Longleftrightarrow {}^6A_{1g}$ Mn^{2+} emission in $RbCdF_3$, τ = 110 msec and X_o = 565 nm, then the value of oscillator strength is $f = 1 * 10^{-8}$.

Only a single green emission band for the Mn^{2+} transitions in $RbCdF_3$ was detected when samples are excited

at 255 nm, 395 nm or 505 nm. The room temperature emission band at peak position of 560 nm has been assigned to the $^4T_{1g}$ (^4G) $\Longleftrightarrow$ $^6A_{1g}$ (^6S) transition (the first excited level to the ground state). The lowest excitation band is situated at about 19685 cm^{-1}, which gives a Stokes shift of 560 nm (17857 cm^{-1}) emission is 1828 cm^{-1}. If we assume hw = 300cm^{-1}, then S = 3. The fact that no zero phonon line was observed suggest the Mn^{2+} is in pure O_h symmetry.

Limited optical studies of Cr^{3+} in $RbCdF_3$ crystal are presented as follows for comparison. A similar test procedure as above was taken. The excitation spectra corresponding to the Cr^{3+} emission in $RbCdF_3$ is presented in Figure 28 (solid line). The observed optical transition energies are assigned to $^4A_{2g}$ $\Longleftrightarrow$ $^4T_{2g}$ (F), $^4T_{1g}$ (F) and $^4T_{1g}$ (P) listed in Table V, and by using the least square method the data are fitted in the Tanabe-Sugano diagram as shown in Figure 29. The crystal field (Dq) and Racah parameters are Dq = 1450 cm^{-1}, B = 780 cm^{-1}, and C/B = 7.

Obviously, the value of crystal field in $RbCdF_3$:Mn^{2+} is less than that of in $RbCdF_3$:Cr^{3+}. This is due to the different charges between two samples. The emission spectrum of Cr^{3+} in $RbCdF_3$ is shown in Figure 28 (dashed line).

Thermal dependence of Mn^{2+} emission in $RbCdF_3$

Figure 25 shows the change in the emission spectra between 77 K and 300 K. The inset presents the manganes emission intensity as a function of temperature in $RbCdF_3$. The emission bands were excited by 505 nm light. The intensity of the luminescence in the range from 10 K to 300K is clearly found to increase linearly as the temperature is raised. The peak position was at 570 nm throughout the temperature region from 10 K to 45 K. A small shift in the peak position is noticeable between 300 K and 10 K (17857 cm^{-1} for 300 K and 17544 cm^{-1} at 10 K).

Temperature dependence of the lifetime of Mn^{2+} fluorescence in $RbCdF_3$

The thermal evolution of the lifetime for the relaxation of $^4T_{1g}$ (^4G) level of Mn^{2+} in $RbCdF_3$ is portrayed in Figure 25. The room temperature measurement yields a value of 62 ms, while a lifetime of 117 ms at 10 K is observed. A constant value of lifetime throughout the temperature region from 10 K to 45 K and then the results corresponding to simple exponential decays are shown as in Figure 26. This suggests that thermalization process is responsible for the decrease in lifetime. The thermalization between energy levels occurs around 77 K. Such a temperature dependence of emission lifetime have been

explained by K. Tanimura and W. A. Sibley (1984),[64] and W. A. Sibley and N. Koumvakalis et al. (1976).[65]

In order to determine if the temperature dependance of Mn^{2+} emmission in $RbCdF_3$ is due to populating another level or to thermal enhancement of the oscillator strength, both the emission intensities (circle) and the value of the reciprocal of lifetime (square) against temperature are plotted in Figure 27. The intensity of Mn^{2+} emission is generally proportional to the τ^{-1}. This tentatively suggests that the oscillator strength as a function of temperature is enhanced in this materials.

TABLE III

ASSIGNMENT OF THE EXCITATION ENERGIES FOR Mn^{2+} TRANSITIONS IN $RbCdF_3$

(THE THEORETICAL VALUES ARE CALCULATED WITH $B = 725\ cm^{-1}$ $D_q = 795\ cm^{-1}$ $C/B = 5\ cm^{-1}$)

TRANSITION	EXPERIMENT	THEORETICAL
$^6A_{1g}$ -- $^4T_{1g}{}^1$	19685 cm^{-1}	19962 cm^{-1}
$^6A_{1g}$ -- $^4T_{2g}{}^1$	23753 cm^{-1}	23289 cm^{-1}
$^6A_{1g}$ -- $^4A_{1g}$, ^4E_g	25445 cm^{-1}	25375 cm^{-1}
$^6A_{1g}$ -- $^4T_{2g}{}^2$	28571 cm^{-1}	28709 cm^{-1}
$^6A_{1g}$ -- $^4E_g{}^b$	30395 cm^{-1}	30450 cm^{-1}

TABLE IV

CRYSTAL FIELD, EMISSION ENERGIES AND LIFETIMES FOR Mn^{2+} IN CRYSTALS AND GLASS AT 80 K

	Crystal field	Racah Parameters		Emission Energy	Lifetime
	Dq (cm^{-1})	B (cm^{-1})	C/B	E (cm^{-1})	τ (msec)
CaF_2	425	770	4.8	20202	180
CdF_2	500	770	4.8	19493	140
ZBLA	630	715	5	17480	44
$RbCdF_3$	795	725	5	17700	90
MgF_2	955	730	5	16580	190

TABLE V

ASSIGNMENT OF THE EXCITATION ENERGIES FOR TRANSITIONS OF Cr^{3+} IN $RbCdF_3$

(THE THEORETICAL VALUES ARE CALCULATED WITH B = 730 cm^{-1} Dq = 1450 cm^{-1} C/B = 7)

TRANSITION	EXPERIMENT	THEORETICAL
$^4A_{2g}$ -- $^4T_{2g}$ (F)	14599 cm^{-1}	14580 cm^{-1}
$^4A_{2g}$ -- $^4T_{1g}$ (F)	21645 cm^{-1}	21410 cm^{-1}
$^4A_{2g}$ -- $^4T_{1g}$ (P)	33113 cm^{-1}	33280 cm^{-1}

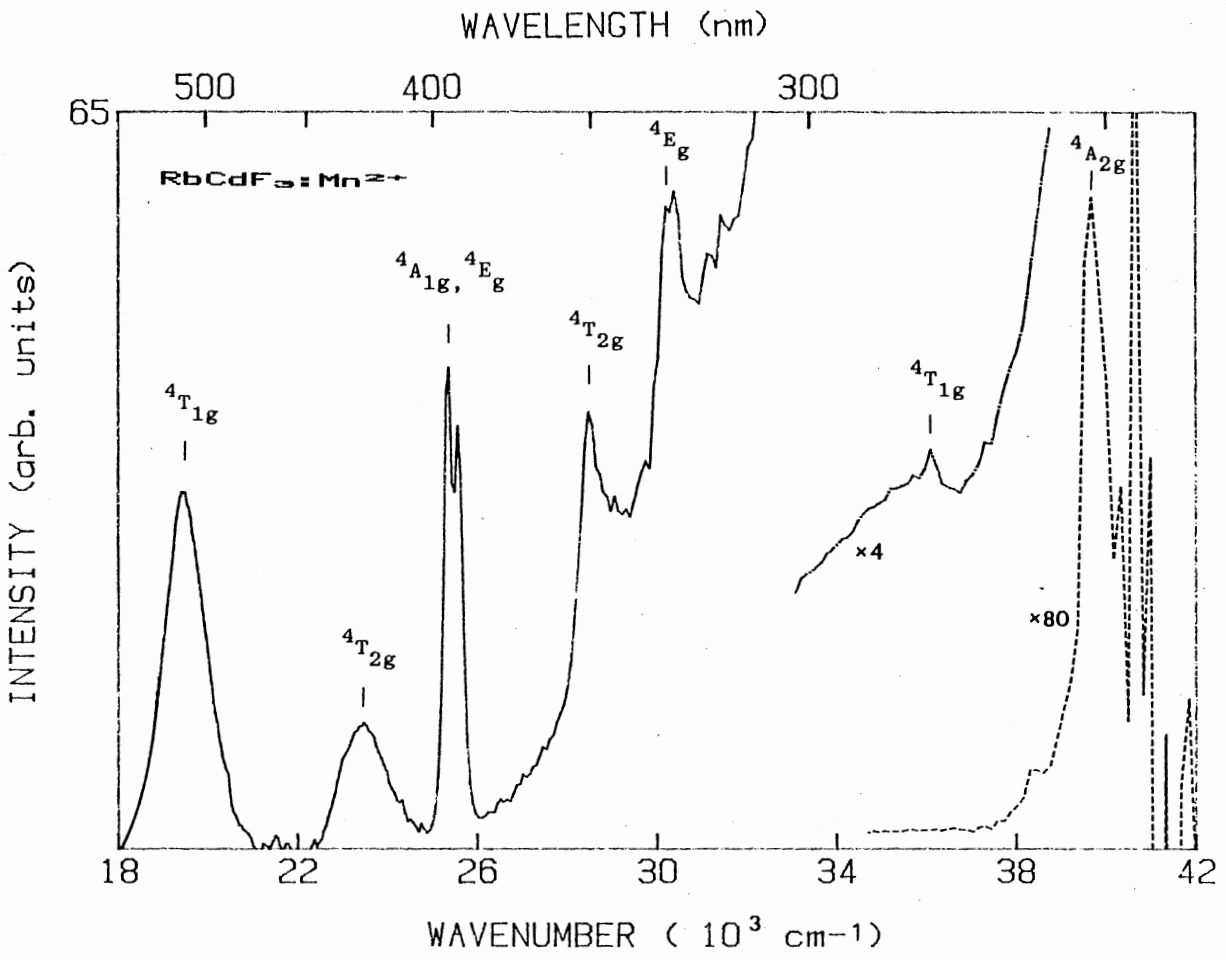

Figure 23. Excitation spectrum of Mn^{2+} ions in $RbCdF_3$ at 10K. Vertical lines show the asign of transition energies

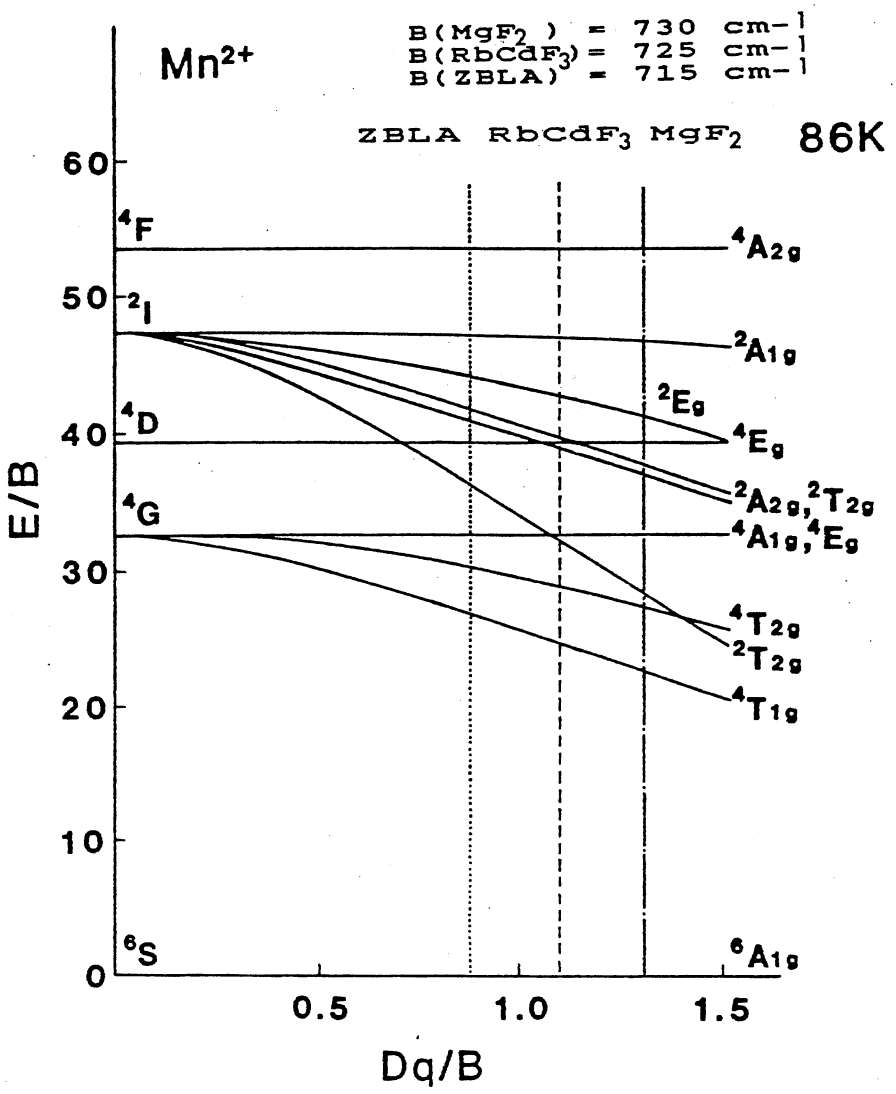

Fig. 24. Tanabe-Sugano diagram for Mn^{2+}. The vertical lines show the normalized crystal fields in $RbCdF_3$ crystal (dashed line), MgF_2 crystal (dash-dotted line) and ZBLA glass(dotted)

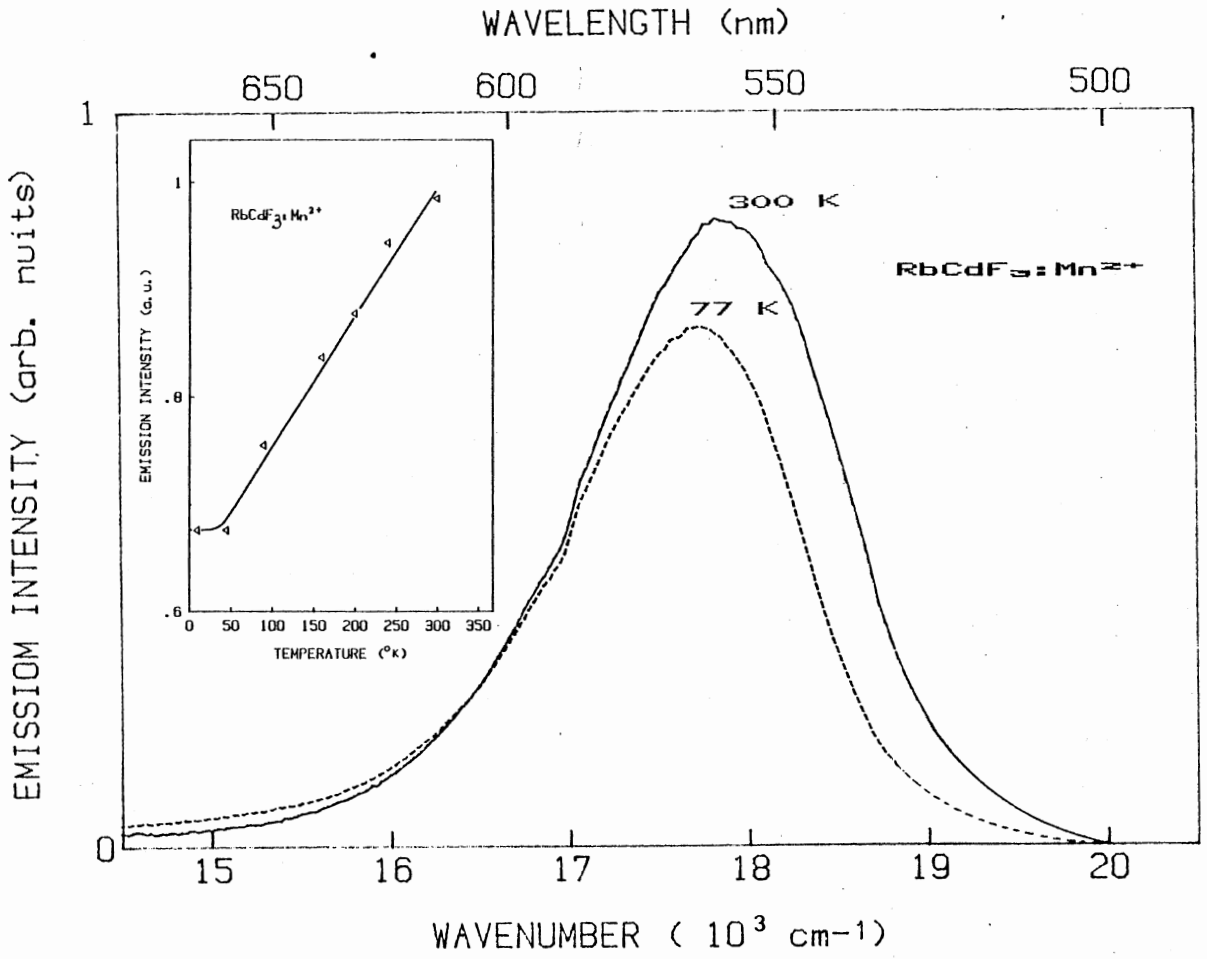

Fig. 25. Emission spectra of Mn^{2+} ions in a $RbCdF_3$ crystal excited at 505 nm at 77K (dashed line) and 300 K (solid line). The inset presents the emission intensities as a function of temperature

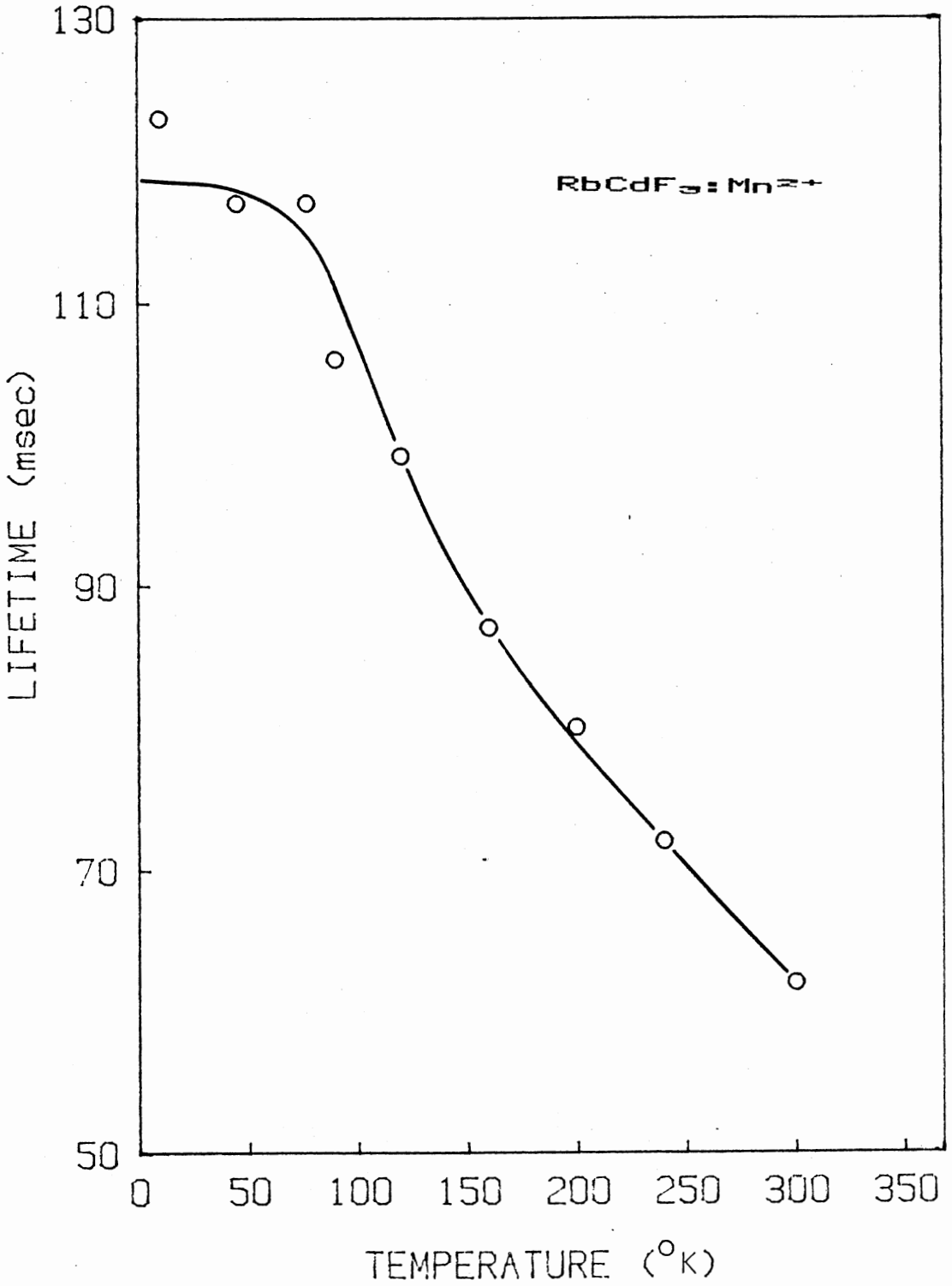

Figure 26. Temperature dependence of Mn^{2+} emission lifetime in $RbCdF_3$ crystal

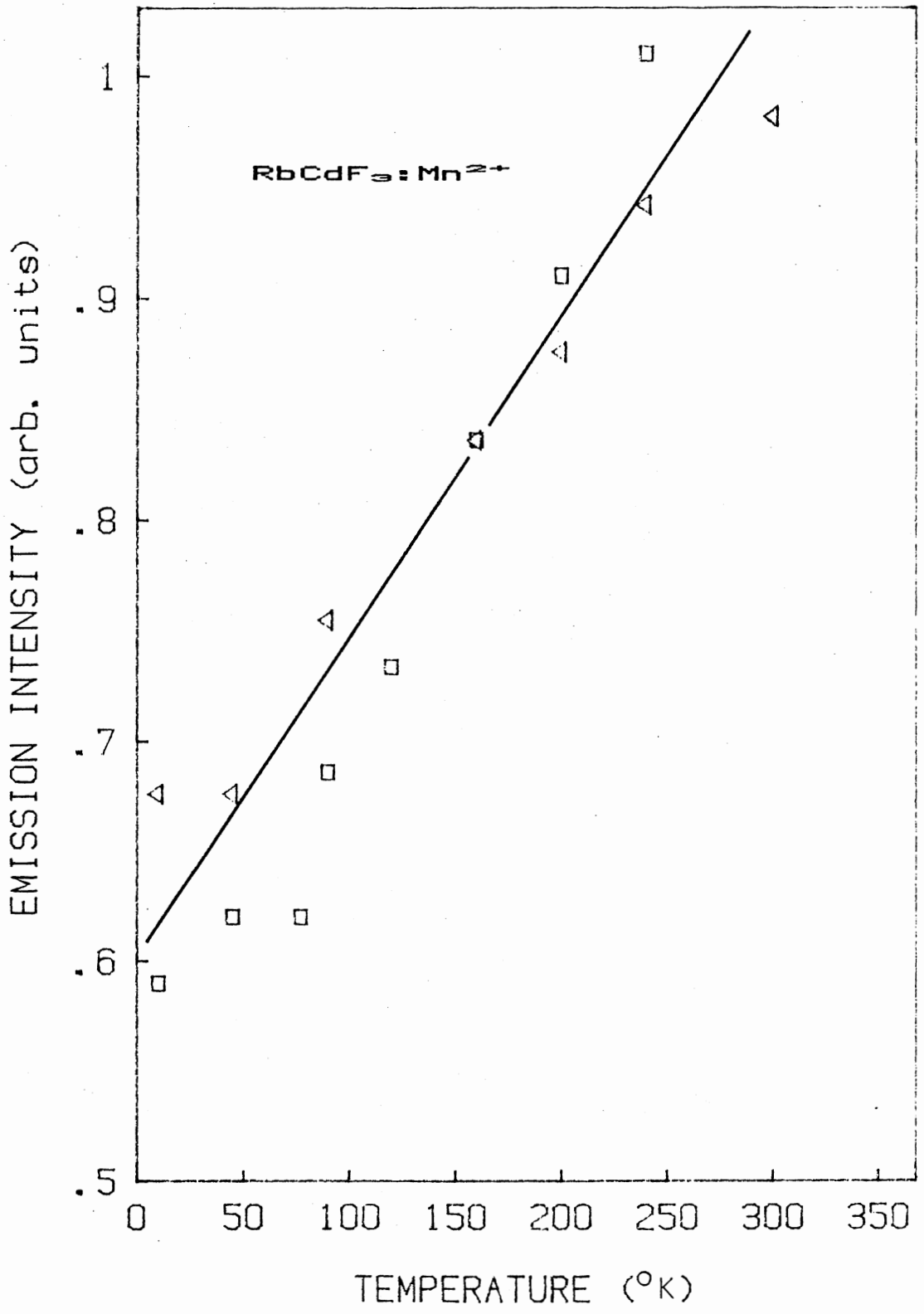

Figure 27. A plot of Mn^{2+} emission intensities and reciprocal of lifetime vs. temperature

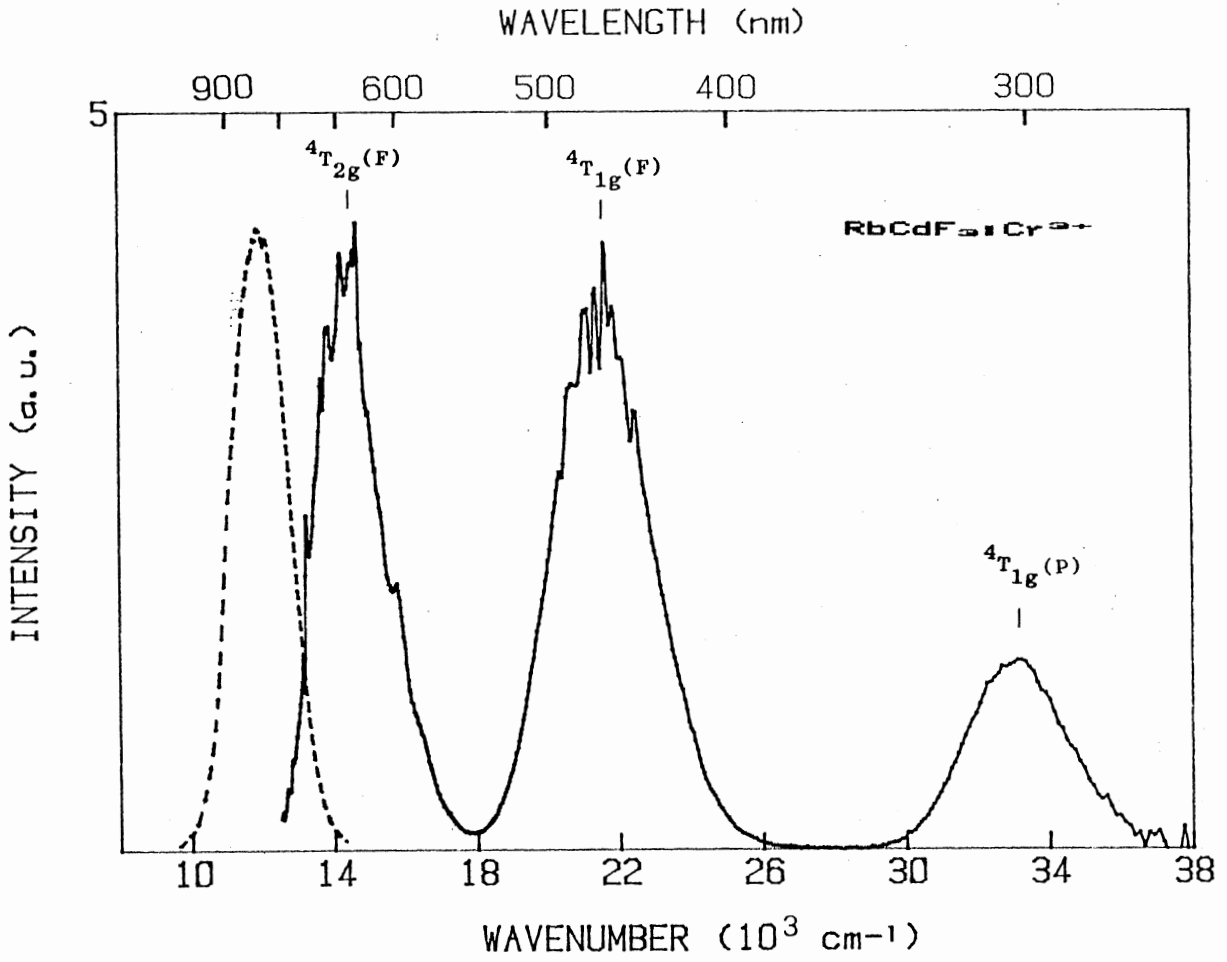

Fig. 28. Emission (dashed line) and excitation(solid line) spectra of Cr^{3+} in $RbCdF_3$ crystal measured at 300 K. The vertical lines show the transition energy assignments

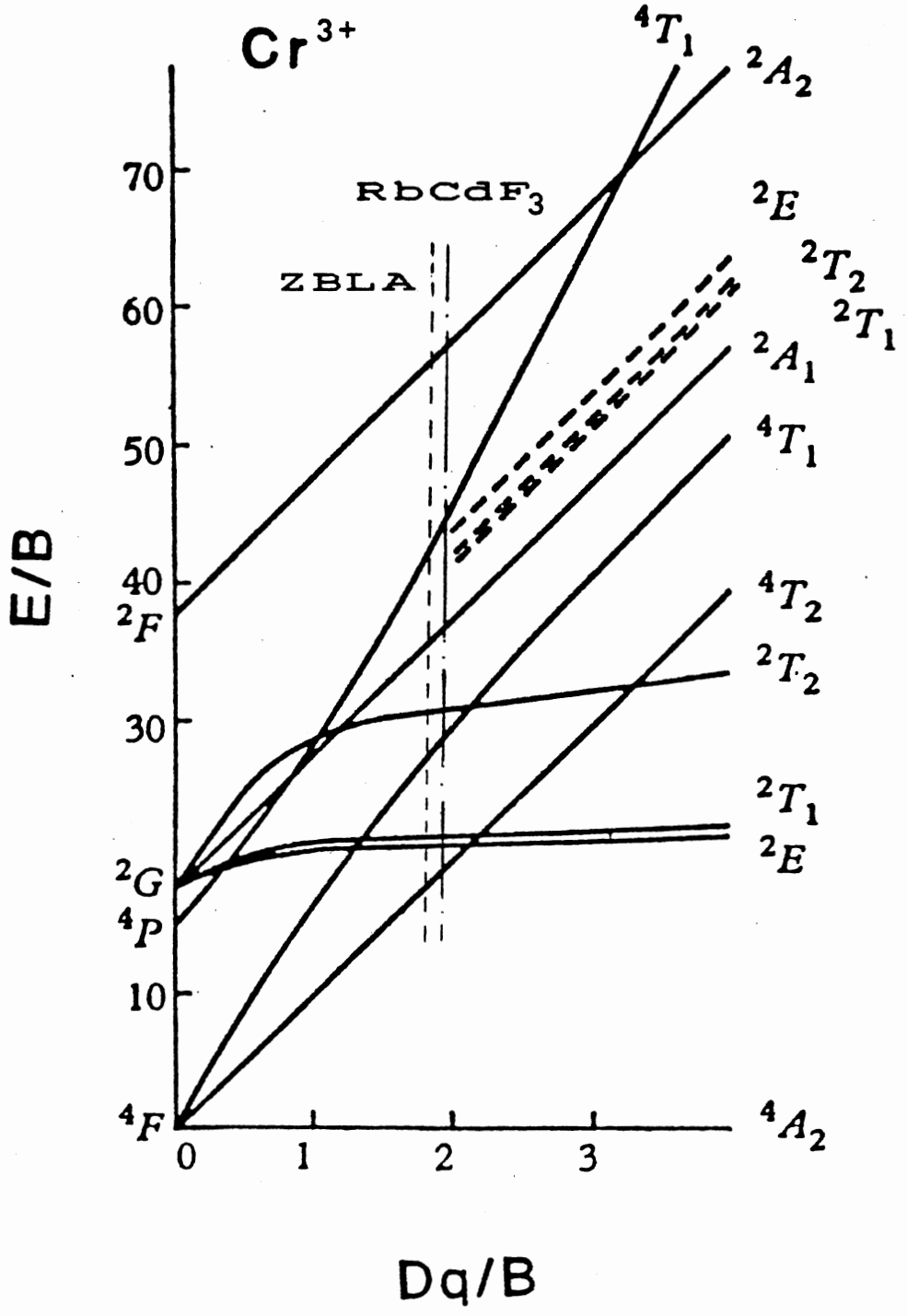

Figure 29. Tanabe-Sugano diagram for Cr^{3+}

CHAPTER V

SUMMARY AND SUGGESTIONS FOR FURTHER STUDY

The present experiments indicate that 77 K electron irradiation produces F-, H-, and V_k-centers in $RbCdF_3$ crystals. The F-center absorption is centered at 286 nm with a 0.68 eV halfwidth, the peak position of the H-band is at 316 nm with a halfwidth of 0.45 eV, and $X_2^-(V_k)$ center absorption is at 365 nm with a 0.57 eV halfwidth at 77 K. The production of H- and F-centers is triggered by the formation of $X_2^-(V_k)$ centers. In Mn^{2+}-doped samples, H-centers are trapped at Mn^{2+}. It is also shown by annealing experiments that there is a loss of the V_k-centers leading to the formation of H- and F-centers in this material. This electron-hole recombination occurs at 260 K for pure $RbCdF_3$, and at 160 K for doped-samples. It is noted that F-centers are not mobile at 300 K.

By comparing the relevant data from the present study for $RbCdF_3$ crystal with those previous results for CaF_2, MgF_2, $RbMgF_3$, $KMgF_3$, $RbCaF_3$, NaCl, KCl, LiF and so on, it can be concluded that the energy of F-band is strongly crystal-dependent as shown in Figure 21. However, for both H- and V_k-bands the peak energy is rather independent.

The emission and excitation spectra of the Mn^{2+} ions in $RbCdF_3$ crystal have been measured. The observed optical transition energies are assigned to $^6A_{1g} \text{---} ^4T_{1g}{}^1$, $^4T_{2g}{}^1$, $^4A_{1g}$ ^4E_g, $^4T_{2g}{}^2$, and $^4E_g{}^b$ by using the least square method to fit data in Tanabe-Sugano diagram. The crystal field (Dq) and Racah parameters are Dq = 795 cm^{-1}, B = 725 cm^{-1}, and C/B = 5 for $RbCdF_3:Mn^{2+}$. The lifetimes of Mn^{2+} ions and the Mn^{2+} emission intensity in this material are observed as a function of temperature.

The following projects are suggested for further study in $RbCdF_3$:

(1) The identification of the extra broad bands absorption which occurs in addition to the 286 nm, 316 nm and 365 nm bands produced by 77 K electron irradiation in pure $RbCdF_3$ may provide further understanding.

(2) A study of F-center mobility in $RbCdF_3$ crystals. From present experimental data, F-centers are not mobile at 300K, and F aggregation is not observed. When annealing to 600 K, a new band of 630 nm appears. This may be due to a Mn^{2+}-radiation defect complex. More work must be done before any definite assignment can be made.

(3) The identification of the 450 nm emission band excited by 300 nm light after electron irradiation of $RbCdF_3$ crystals. This 450 nm emission band was observed both before and after electron irradiation in pure $RbCdF_3$ and $RbCdF_3:Mn^{2+}$ from this experiment. A further study of the

band in unirradiated samples would provide more information about optical properties in this material.

(4) A polarization study of emission and excitation spectra of Mn^{2+} ion in $RbCdF_3$.

REFERENCES

1. Arecchi, F. T. and E. O. Schulz-Dubois,"Laser Handbook" (North-Holland, 1972).

2. Sibley, W. A. and Derek Pooley, "Radiation Studies of Materials Using Color Centers" (Academic Press, New York 1974).

3. Brice, J. C., "The Grewth of Crystals From the Melt" (Nroth Holland Prbl.Co., Amsterdam), 1965.

4. Billington, D. S., " Radiation Damage in Solids " (Academic Press, New York 1962).

5. Van Doorn, C. Z., Rev. of Sci. Instr., 32, 755 (1961).

6. Seitz, F., Rev. Mod. Phys., 18, 384 (1946).

7. Seitz, F., Rev. Mod. Phys., 26, (1954).

8. Gruber, B., " Theory of Crystal Defects " 339 (1966, Academic Press, New York).

9. Kircher, John F. and R. E. Bowman,"Effects of Radiation on Materials and Components" (Reinhold Publishing Corporation, New York 1964).

10. Schulman, J. H. and W. D. Compton, " Color Center in Solids " (Pergamon, N. Y. 1971).

11. Fowler, W. B., "The Physics of Color Centers" (Academic Press, N. Y., 1968).

12. Crawford, J. H., Advan. Phys. 17, 93 (1968).

13. De Boer, J. H., Receuil Trav. Chem. Phys-Bus 56, 301 (1937).

14. Castner, T. G., and W. Kanzig, J. Phys. Chem. Solids 3, 178 (1957).

15. Daly, D. F. and R. L. Micher, Phys. Rev. Letters 19, 637 (1967); Phys. Rev. 175, 412 (1968).

16. Kanzig, W. and T. O. Woodruff, J. Phys. Chem. Solids 9, 70 (1958).

17. Varley, J. H. O. Nature 174, 886 (1954); F. Nuclear Energy 1, 130 (1954).

18. Itoh, N. ," Defects In Insulating Crystals ", edited by V. M. Tuchkevich and K. K. Shvarts (Springen-Verlog, Berlin, 1981), 343, and J.de Physique 37,C7-27(1976).

19. Williams, R. T. and M. N. Kabler, Phys. Rev. B9, 1897 (1974).

20. Williams, R. T., Semiconductors and Insulators, 3, 251 (1978).

21. Toyozawa, T., Solid State Electronics, 21, 1313,(1978).

22. Williams, R. T., Phys. Rev. Letters, 36, 529, (1976).

23. Leung, C. H. and K. S. Song, Phys. Rev. B18, 922(1978).

24. Soda, K. and N. Itoh, J. Phys. Soc. Japan, 48, 1618, (1980).

25. Williams, R. T., M. N. Kabler, and I. Schneider, J. Phys. C., 11, 2009, (1978).

26. Williams, R. T., J. N. Bradford, and W. L. Faust, Phys. Rev., B18, 7038, (1978).

27. D'hertoghe, J. and G. Jacobs, Phys. Stat. Sol. (b) 95, 291, (1979).

28. Ortega, J. M., Phys. Rev., B19, 3222, (1979).

29. Suzuki, Y., M. Okumura and M. Hirai, J. Phys. Soc. Japan, 47, 184, (1979).

30. Williams, R. T., C. L. Marquardt, J. W. Williams, and M. N. kabler, Phys.Rev., B15, 5003, (1977).

31. Sibley, W. A., E. Sonder, and C. T. Butler, Phys. Rev. 136, A537, (1964).

32. Tanimura and T. Okada, Phys. Rev., B21, 1690, (1980).

33. Roussean, M., Phys. Rev.B, Vol.12, #4, 12, 1579,(1975).

34. Rousseat, J. J., Phys. Stat. Sol. (b), 73, 625, (1976).

35. Flocken, J. W., Ferroelectrics, Vol.55, 125-128,(1984).

36. Studzinski, P. and J. M. Spaeth, " Lattice Defects In

Iron Crystals ", Dublin, Ireland, (1982).

37. Halliburton, L. E. and K. L. Sweeney, Nuc. Instru. & Methods In Phys. Research B1, 344-347, (1984).

38. Butler, L. T., Phys. Rev. (1967).

39. Feuergelm, L. N., Ph.D Thesis, (O. S. U. 1980).

40. Riley,C. R. and W. A. Sibley, Phys. Rev. B1 1789(1970).

41. Riley, C. R., S. I. Yun and W. A. Sibley, Phys. Rev. B5, 3285 (1972).

42. Lewis, J. T., J. L. Kolopns, E. Sonder and M.M. Abraham Phys. Rev., B7, 810, (1973).

43. Alcala, R., N. Koumnakalis, W. A. Sibley, Phys. St. Solidi, (a)30, 449, (1975).

44. Vehse, W. E. and W. A. Sibley, Phys. Rev., B6, 2443, (1972).

45. Hills, M. E. and W. R. McBride, J. Chem. Phys., 40, 2053, (1964).

46. Blunt, R. F. and M. I. Cohen, Phys. Rev., 153, 1031, (1967).

47. Facey, O. E. and W. A. Sibley, Phys. Rev., 174, 1076, (1968).

48. Facey, O. E. and W. A. Sibley, Phys. Rev., B2, 1111, (1970).

49. Smakula, A., Z. Phys., 59, 603, (1930).

50. Dexter, D. L., Phys. Rev., 101, 48, (1956).

51. Itoh, N. and M. Saidoh, Phys. Stat. Sol., 33, 649, (1969).

52. Itoh, N., B. S. H. Royce and R. Smoluchowski, Phys.Rev. 13, 1766, (1965).

53. Itoh, N. and B. S. H. Royce, J. Phys. Chem. Solids, 27, 1366, (1966).

54. Kilck, C. C. and J. H. Schulman, J. Opt. Soc. Amer. 42, 910, (1952).

55. Koumvakalis, N., W. A. Sibley and G. E. Venikuoas, J. Lumin., 15, 283, (1977).

56. Alonso, P. J. and R. Alcala, J. Lumin., 22, 321,(1981).

57. Feuerhelm, L. N., S. M. Sibley and W. A. Sibley, J. Solid State Chem., 54, 164-169, (1984).

58. Stevels, A. L. N., J. Lumin., 20, 99-109, (1979).

59. Lanver, U. and G. Lehmann, J. Lumin., 17, 225-235, (1978).

60. Tanabe, Y. and S. Sugano, J. Phys. Soc. Japan, 9, 753-766, (1954).

61. Suzuki, Y. and W. A. Sibley,

62. Alonso, P. J. and R. Alcala, J. Lumin., 22, 321-333, (1981).

63. Dibartolo, B., "Optical Interactions in Solids", Wiley, New York, (1968).

64. Tanimura, K. and W. A. Sibley, Amer. Phys. Soc., 31, 3980, (1984).

65. Sibley, W. A. and N. Koumvakalis, Phys. Rev. B, 14, 35, (1976).

VITA 2

Ruo-Ling Hu

Candidate for the Degree of

Master of Science

Thesis: OPTICAL STUDIES OF RADIATION DAMAGE AND IMPURITIES IN $RbCdF_3$

Major field: Physics

Biographical:

Personal Data: Born in Shanghai, China, the daughter of Ji-Deng Hu and Wan-Zheng Zhu. Married.

Education: Graduated from the 55th High School, Shanghai, China, in June, 1961; received Bachelor of Science Degree in Engineering from Shanghai Institute of Mechanical Engineering in June, 1966; completed requirements for the degree of Master of Science at Oklahoma State University in July, 1987.

Professional Experience: Engineer, Hanjiang Precision Machine Tool Research Institute, Hanzhong, China. Teaching Assistant and Research Assistant, Department of Physics, Oklahoma State University, August,1984, to May, 1987.